



HAL
open science

SURF2 is a MDM2 antagonist in triggering the nucleolar stress response

Sophie Tagnères, Paulo Espirito Santo, Julie Radermecker, Dana Rinaldi, Carine Froment, Quentin Provost, Manon Bongers, Solemne Capeille, Nick Watkins, Julien Marcoux, et al.

► To cite this version:

Sophie Tagnères, Paulo Espirito Santo, Julie Radermecker, Dana Rinaldi, Carine Froment, et al.. SURF2 is a MDM2 antagonist in triggering the nucleolar stress response. *Nature Communications*, 2024, 15 (1), pp.8404. 10.1038/s41467-024-52659-x . hal-04739145

HAL Id: hal-04739145

<https://hal.science/hal-04739145v1>

Submitted on 21 Oct 2024

HAL is a multi-disciplinary open access archive for the deposit and dissemination of scientific research documents, whether they are published or not. The documents may come from teaching and research institutions in France or abroad, or from public or private research centers.

L'archive ouverte pluridisciplinaire **HAL**, est destinée au dépôt et à la diffusion de documents scientifiques de niveau recherche, publiés ou non, émanant des établissements d'enseignement et de recherche français ou étrangers, des laboratoires publics ou privés.

SURF2 is a MDM2 antagonist in triggering the nucleolar stress response

Received: 21 November 2023

Accepted: 16 September 2024

Published online: 27 September 2024

 Check for updates

Sophie Tagnères¹, Paulo Espirito Santo¹, Julie Radermecker², Dana Rinaldi¹, Carine Froment^{3,4}, Quentin Provost¹, Manon Bongers¹, Solemne Capeille¹, Nick Watkins⁵, Julien Marcoux^{3,4}, Pierre-Emmanuel Gleizes¹, Virginie Marcel², Célia Plisson-Chastang¹ & Simon Lebaron^{1,6} ✉

Cancer cells rely on high ribosome production to sustain their proliferation rate. Many chemotherapies impede ribosome production which is perceived by cells as “nucleolar stress” (NS), triggering p53-dependent and independent pathways leading to cell cycle arrest and/or apoptosis. The 5S ribonucleo-protein (RNP) particle, a sub-ribosomal particle, is instrumental to NS response. Upon ribosome assembly defects, the 5S RNP accumulates as free form. This free form is able to sequester and inhibit MDM2, thus promoting p53 stabilization. To investigate how cancer cells can resist to NS, here we purify free 5S RNP and uncover an interaction partner, SURF2. Functional characterization of SURF2 shows that its depletion increases cellular sensitivity to NS, while its overexpression promotes their resistance to it. Consistently, SURF2 is overexpressed in many cancers and its expression level is an independent marker of prognosis for adrenocortical cancer. Our data demonstrate that SURF2 buffers free 5S RNP particles, and can modulate their activity, paving the way for the research of new molecules that can finely tune the response to nucleolar stress in the framework of cancer therapies.

Cancers originate from the accumulation of genetic events that allow uncontrolled cell proliferation. Thanks to large-scale sequencing of the cancer genome, it is now possible to identify cancer-specific alterations. This information can then be used for diagnosis but also allows the development of alternative therapeutic approaches for specific targets¹. Although these so-called targeted therapies have proven to be effective, they are also associated with side effects that hinder their advantages. Moreover, drug resistance, induced either by mutation of the specific target or the activation of alternative survival pathways, is often observed². Combination therapies are therefore needed to modulate the metabolic circuits that support the proliferation of cancer cells. A key metabolic pathway in cancer cells is the abnormal

boost in ribosome synthesis to meet the protein requirements associated with uncontrolled cell growth and proliferation³. The nucleolus is the nuclear sub-compartment where ribosome synthesis begins, and the boost in ribosome synthesis is associated with increased nucleolus size. This phenotype has long been used as a marker of tumor cell aggressiveness^{3,4}. Certain cancer types and cancer cell populations are thus addicted to ribosome synthesis.

Nucleolar stress (NS) can be defined as any stress leading to the inhibition of ribosome assembly, a complex and energy-consuming process that begins with the transcription of ribosomal DNA by the specific RNA polymerase I (Pol I) in the nucleolus⁵. Under stress, cells reduce ribosome production to conserve energy and stop cell

¹Molecular, Cellular and Developmental Biology unit (MCD), Centre de Biologie Intégrative (CBI), Team with an accreditation from the French “Ligue contre le Cancer” organism., University of Toulouse, CNRS, UPS, 118 route de Narbonne, Toulouse, Cedex, France. ²Centre de Recherche en Cancérologie de Lyon, Inserm U1052, CNRS UMR5286, Université de Lyon, Université Claude Bernard Lyon 1, Centre Léon Bérard, CEDEX 08, Lyon, France. ³Institut de Pharmacologie et de Biologie Structurale (IPBS), Université de Toulouse, CNRS, Université Toulouse III-Paul Sabatier (UPS), Toulouse, France. ⁴Infrastructure Nationale de Protéomique, ProFI, Toulouse, France. ⁵Biosciences Institute, The Medical School, Newcastle University, Newcastle upon Tyne, UK. ⁶Institut national de la santé et de la recherche médicale (INSERM), Paris, France. ✉e-mail: simon.lebaron@univ-tlse3.fr

proliferation⁶. These cell-specific regulations of ribosome synthesis are thus essential to the control of cell growth in all living cells. Nevertheless, mature ribosomal subunits are stable entities, so the inhibition of their synthesis will only affect cellular protein homeostasis after long-term exposure to stress. In addition to these long-term regulations, ribosome synthesis shutdown upon stress signaling is directly linked to cell cycle arrest^{7,8}. In humans, this is induced by stabilization and activation of the tumor suppressor p53^{7,9–13}. This pathway is prevalent in the regulation of p53 under normal and pathological conditions^{14–16}. Several ribosomal proteins have been described as being able to mediate such p53 regulation in response to stress. The general idea is that ribosomal proteins that are released from or not integrated into ribosomes can accumulate as the free form in the nucleoplasm. There, they can directly bind MDM2 and inhibit its ubiquitinylase activity^{17–21}. Such a role for ribosomal proteins has been generally termed an extra-ribosomal function. However, among the different ribosomal proteins that support such regulation of p53 activation, only RPL5 and RPL11 are instrumental to this response. Interestingly, both proteins are components of the same complex, the 5S ribonucleoprotein (RNP) particle.^{14,22–24} 5S RNPs consist of the association of 5S ribosomal RNA (rRNA) with the ribosomal proteins RPL5 and RPL11. These particles are largely incorporated into nascent large/60S ribosomal subunits. Disruption of ribosome synthesis results in the accumulation of so-called free 5S RNPs in the nucleoplasm. Free 5S RNPs interact with the E3-ubiquitin ligase MDM2 and inhibit its activity. MDM2 normally targets p53 to the proteasome for degradation, so free 5S RNPs promote stabilization and activation of p53^{14,22}. Importantly, NS does not result in p53 stabilization and activation in the absence of 5S RNP components, demonstrating that 5S RNPs play a critical role in the NS response^{14,22}. It appears that altering the balance in favor of 5S RNP integration into ribosomes will contribute to cancer development and therapeutic resistance²⁵. Thus, promoting the extra-ribosomal activity of free 5S RNPs in cancers with wild-type TP53 may improve the p53-dependent anticancer effects of the chemotherapy used in poor prognosis cancers. On the other hand, little is known about the putative existence of a free 5S RNP pool under basal conditions. Given that 5S rRNA is independently transcribed by RNA polymerase III instead of RNA polymerase I for the other rRNAs, a logical hypothesis would be that 5S rRNA production is not in complete stoichiometry with other ribosomal RNAs, even under basal conditions.

Many cancer treatments that are not purposefully designed to target ribosome synthesis induce an NS response, including chemotherapies^{14,16,26}. Even though ribosome synthesis is essential in all living cells, cancer cells are more sensitive to its inhibition. Indeed, ribosome synthesis is strongly increased in cancer cells, which requires a greater synthesis of all its components, including 5S RNPs. When this process is altered, a greater amount of free 5S accumulates, thus mediating a stronger p53 activation²⁷. This phenomenon partly explains why cancer cells are more sensitive to nucleolar stress than normal^{28,29}. Therefore, activation of the NS response by anticancer drugs such as 5-fluorouracil (5-FU) or doxorubicin contributes to their therapeutic benefit²⁶. However, as frequently observed for many cancer treatments, in clinical trials using a new class of Pol I transcription inhibitors, half of the patients showed progressive disease, indicating that resistance mechanisms may be occurring³⁰. However, how cancer cells resist NS in wild-type TP53 tumor patients remains to be understood.

In order to better understand how free 5S RNP can influence cell fate (ie, cell survival or death) under nucleolar stress conditions, we purified these particles to find partners that could regulate their activity. We identified the protein SURF2 as a faithful interactant of free 5S RNP particles. Our results demonstrate that SURF2 buffers the activity of free 5S RNP particles in basal conditions to avoid unnecessary activation of the nucleolar stress response. However, SURF2 counteracts p53 activation after NS, hence its expression is

upregulated in many cancers and negatively correlates with the survival of patients suffering from adrenocortical cancer. Our comprehensive dataset supports a model in which SURF2 competes with MDM2 for their association to free 5S RNPs, and their alternative binding thus modulates the response to nucleolar stress. Inhibition of SURF2 may be a promising therapeutic avenue to promote both p53-dependent and independent nucleolar stress responses.

Results

SURF2 is a binding partner of free 5S RNP particles

To identify potential regulators of free 5S RNPs, we set out to purify these particles outside the ribosomes. 5S particles are formed by the association of the 5S rRNA, with the ribosomal proteins RPL5 and RPL11, whether they are integrated into the ribosome or accumulate as independent particles. We, therefore, developed a U2OS cell line known to respond well to NS, that inducibly overexpresses RPL5-Flag using Flip-In T-REx constructs (Supplementary Fig. S1). We verified the expression of RPL5-Flag and used sucrose gradient fractionation to confirm that the fusion protein accumulates in both ribosomal and free fractions without altering ribosomal subunit production (Supplementary Figs. S1A, S1B). We also verified its lack of impact on the process of ribosome assembly, which consists of the maturation of a large primary transcript that contains mature rRNA sequences (18 S, 5.8 S, and 28 S) separated by spacers that are removed after exo- and endo-nucleolytic steps. rRNA processing occurs inside pre-ribosomal particles constituted of pre-rRNAs associated with both ribosomal proteins and transiently associated factors, the latter being absent from mature ribosomal subunits (Supplementary Fig. S1C)^{5,31}. Disruption of ribosome assembly will lead to abnormal accumulation of rRNA precursors and reduced rRNA production^{32–34}. To confirm that ectopic expression of RPL5-Flag did not affect ribosome synthesis and maturation, we assessed pre-rRNA processing using northern blots (Supplementary Fig. S1D). No changes in the accumulation of rRNA precursors nor mature forms were observed, indicating that RPL5-Flag expression does not perturb ribosome assembly.

To enrich partners of the free 5S RNP, ribosomes and pre-ribosomes were separated through a sucrose cushion. Free 5S RNP particles were purified from the supernatant, using RPL5-Flag and beads coupled with anti-Flag antibodies (Supplementary Fig. S1E). Interacting proteins were recovered, digested with trypsin and analyzed by nano-liquid chromatography-tandem mass spectrometry (nanoLC-MS/MS) using differential label-free quantitative proteomics (Fig. 1). To evaluate interaction changes, pairwise comparison based on MS intensity values was performed for each quantified protein, first, between RPL5-Flag-expressing cells and control U2OS cells only expressing the Flag-tag (Fig. 1a). Enriched proteins were selected based on their significant protein abundance variations between the two compared conditions (fold-change (FC) > 2 and < 0.5, and Student *t* test *p*-value < 0.05) (see material and methods for details). The volcano plot presented in Fig. 1a shows that several proteins were significantly co-purified with RPL5-Flag, indicating them as potential partners of free 5S RNP (Fig. 1a and Supplementary Table S1). RPL11, the other component of the 5S RNP particles, was found with a similar fold-change (FC = 33.34) compared to the RPL5-Flag bait (FC = 59.3), confirming the efficient purification of the 5S particles and that RPL5-Flag is mainly in complex with RPL11. No other ribosomal proteins were found specifically enriched in this purification, attesting to the efficiency of the ribosomal fraction elimination step.

We also found MDM2 (FC = 58.01), already described as a major free 5S RNP partner^{22,35–37}. SSB/La-protein, a known chaperone of newly synthesized 5S rRNA, is also enriched as well as HEATR3, a chaperone of RPL5^{14,38–42}. The presence of p53 was not anticipated but might correspond to an indirect interaction via MDM2. We tested this hypothesis by using Nutlin-3a, a p53 interaction inhibitor that targets MDM2 binding pocket⁴³ (Supplementary Fig. S2). During these

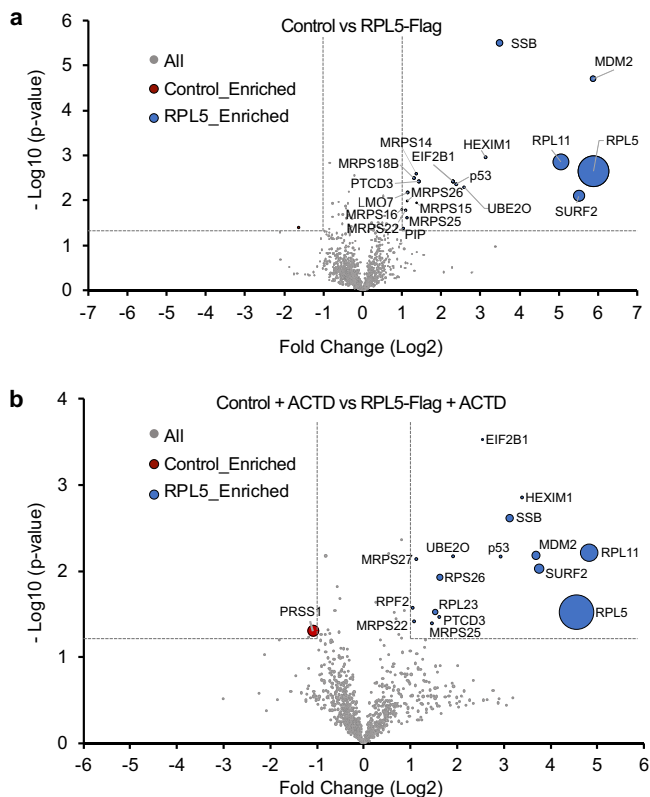


Fig. 1 | Label-free quantitative proteomics analysis of RPL5-FLAG co-purified proteins. Nano-liquid chromatography-tandem mass spectrometry (nanoLC-MS/MS) analysis of trypsin digested proteins retained on flag-coated beads issued from U2OS control cells (LEFT quadrant) or cell expressing RPL5-FLAG (RIGHT quadrant). Three independent experimental replicates ($n = 3$) were performed. Volcano plots showing proteins significantly enriched for control cells (red) versus cells expressing RPL5-FLAG (a) in untreated cells (b) in cells treated with actinomycin D (ACTD, 10 ng/ml) for 24 h. An unpaired two-tailed Student's t test with equal variance was used. Enrichment significance thresholds are represented by an absolute \log_2 -transformed fold-change (FC) greater than 1 and a $-\log_{10}$ -transformed (p -value) greater than 1.3. The iBAQ (intensity-Based Absolute Quantification) values are represented by the diameter of each dot for the proteins that are significantly enriched in order to rank their absolute abundances⁷³. Source data are provided as a Source Data file.

experiments, we could reproduce our previous results showing an interaction between p53 and free 5S RNP using IPs followed by western-blot analysis (Supplementary Fig. S2). However, this association is lost in the presence of Nutlin-3a. This observation demonstrates that the binding of MDM2 to free 5S RNP and p53 are not mutually exclusive in U2OS cells.

HEXIM1 was also significantly enriched (FC = 8.75) during this experiment, but we could not reproduce this interaction using HEXIM1 as a bait during a reverse IP experiment. Of interest, SURF2 was significantly and highly enriched (FC = 45.69) during RPL5-Flag purification (Fig. 1a). Other proteins such as mitochondrial ribosomal proteins (MRPS14, MRPS15, MRPS16, MRPS18B, MRPS22, MRPS25, and MRPS26); UBE20 (a ubiquitin-ligase protein) and EIF2B1 (translation initiation factor) were also specifically found albeit with reduced fold-changes compared to other partners. To investigate how the panel of free 5S RNP binding partners changes during stress, we used the same purification strategy but this time after inducing NS with a low dose of actinomycin D (ACTD) (10 ng/mL for 24 h) (Fig. 1b). The repertoire of potential free RPL5-flag partners showed few changes, with only increased enrichment of MDM2 (Fig. 1b and Supplementary Table S2).

Among RPL5-Flag partners, SURF2 stood out, both as an abundant (areas of circles are proportional to the iBAQ abundance of each

protein) and strongly enriched before or following NS induction (FC = 45.69 and 14.42, respectively). Indeed, it is the second most enriched partner of RPL5-Flag in both normal and NS conditions. SURF2 (Surfeit Locus 2) shares a c-Myc responsive promoter with SURF1, located in a crowded and conserved region^{44–46}. We found almost no functional data for SURF2. However, the genomic region contains other genes encoding for factors involved in ribosome production (SURF3/RPL7A and SURF6/RRP14), a transmembrane receptor involved in endoplasmic reticulum export (SURF4), a component of the mediator complex (SURF5/MED22) and a factor involved in cytochrome-c synthesis (SURF1/SHY1), all of which promote cell growth and proliferation. To understand what role SURF2 might play in relation to free 5S RNP particles, we undertook its characterization in U2OS cells.

SURF2 binds 5S RNP particles but is not involved in ribosome assembly

Free 5S RNP particles are normally incorporated into ribosomes, so we tested whether SURF2 was involved in this process. SURF2 is described in the human protein atlas as a nucleoplasmic and nucleolar component, suggesting a potential role in ribosome assembly (<https://www.proteinatlas.org/ENSG00000148291-SURF2>). SURF2 was purified from U2OS whole cell extract by immunoprecipitation using anti-SURF2 antibodies, with anti-GAPDH as a control. Protein partners were identified by a differential label-free quantitative proteomics approach and shown in a volcano plot (Fig. 2a). As expected, RPL5 and RPL11 were significantly enriched with SURF2 (Fig. 2a, b and Supplementary Table S3). Among other factors identified, TRIM21 and PRDX1 are common contaminants from U2OS extracts (see CRAPome database)⁴⁷, while DLST (dihydrolipoamide S-succinyltransferase) is mitochondrial, and these were not considered further. RPF2 and RRS1, which mediate proper integration of 5S RNP particles to pre-60S pre-ribosomal subunits, were identified^{42,48–50}. Their low abundance could reflect a transient interaction of these proteins with free 5S RNP particles before being integrated into ribosomes (Fig. 2b). Of notice, no other ribosomes-associated proteins were significantly co-purified with SURF2, supporting an absence of SURF2 function in ribosome synthesis.

To test whether SURF2 interaction with RPL5 and RPL11 occurs inside or outside of free 5S RNP particles, we tested the interaction of SURF2 with RNAs in the cell by performing IP using either beads coupled to anti-SURF2, anti-HEXIM1 (HEXIM1 being found associated with RPL5-Flag, see Fig. 1 above) or beads not coupled with antibodies (termed “beads” in Fig. 2) as control experiment. RNAs enriched during the IPs in the different conditions were labeled with P³² using pCp labeling and separated on a polyacrylamide gel (Fig. 2c). HEXIM1 specifically enriched its known RNA partner 7SK, but no other RNAs under normal or NS (actinomycin D treatment) conditions. In contrast, SURF2 retained significantly more 5S rRNA than control beads in both normal and NS conditions, indicating that SURF2 specifically interacts with 5S rRNA in addition to RPL5 and RPL11. Interestingly, 5.8S rRNA, which only exists in the cell in the mature 60S ribosomal subunits, was not enriched during these experiments, suggesting again that SURF2 does not interact with mature ribosomes. To confirm that SURF2 only interacts with 5S RNP particles in their free form, we performed a cell fractionation analysis using the recently developed Pre-ribosome Sequential Extraction (PSE) method⁵¹ (see material and methods) (Fig. 2d). Localization of SURF2 in different cell fractions (cytoplasmic/nuclear and nucleolar fractions) was tested by western-blot and compared to other proteins. SURF2 was preferentially enriched in the cytoplasmic/nuclear fraction, as observed for p53, while RPL5, RPL11, and RPL17 are equivalently present in nucleolar fractions. This indicates that SURF2 preferentially localizes outside the nucleoli, where initial steps of ribosome synthesis occur, indicating that it does not interact with early pre-ribosomes. To confirm this conclusion, we localized SURF2 using microscopy. Despite being efficient for western blot and IPs, anti-SURF2

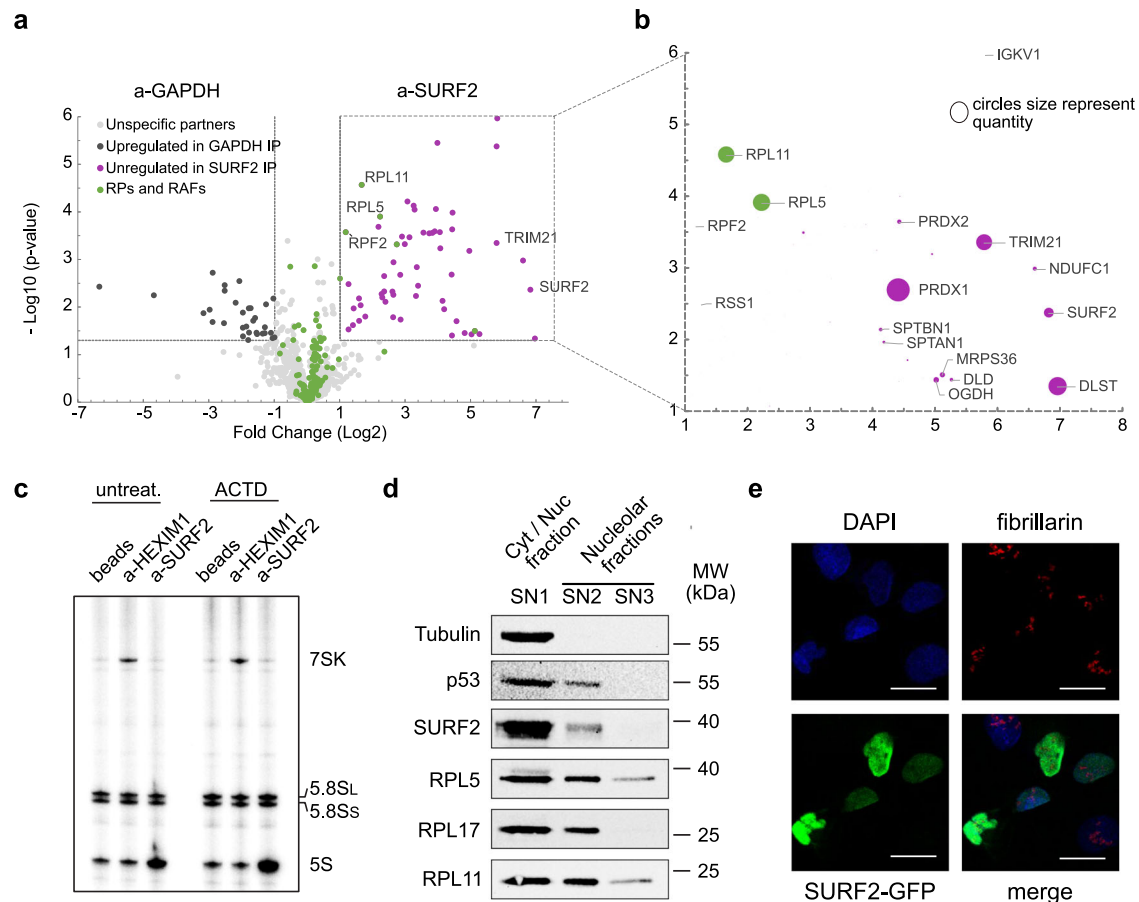


Fig. 2 | SURF2 is a partner of free 5S particles and is involved in p53 regulation.

a Label-free quantitative proteomics analysis of trypsin-digested proteins retained on beads coated by anti-GAPDH or anti-SURF2 antibodies. Three independent experimental replicates ($n = 3$) were performed. Volcano plot showing proteins significantly enriched in the GAPDH IP (brown) versus the SURF2 IP (purple). An unpaired two-tailed Student's t test with equal variance was used. Enrichment significance thresholds are represented by an absolute \log_2 -transformed fold-change (FC) greater than 1 and a $-\log_{10}$ -transformed (p -value) greater than 1.3. Proteins involved in ribosome biogenesis and function are indicated in green. **b** Focus on the iBAQ values, represented by the diameter of each dot, for the proteins significantly enriched in the SURF2 IP. **c** Detection of RNAs associated with HEXIM1 and SURF2. U2OS RNAs co-immunoprecipitated with endogenous HEXIM1 (a-HEXIM1) or

endogenous SURF2 (a-SURF2) were 3'-labeled and separated on a 6% acrylamide gel. Control IP reaction performed without antibodies (beads) is shown ($n = 1$). **d** U2OS cell extracts were fractionated using the PSE method. Western-blot analyses showing the contents of different factors (indicated at the left of the gel) in the SN1, SN2, and SN3 fractions obtained with the PSE method ($n = 2$). **e** Microscopy analyses of U2OS cells over-expressing SURF2-GFP from TET inducible promoter. Cells were induced with tetracycline to obtain a similar expression as the endogenous copy (tetracycline at 5 ng/mL), and a SURF2-GFP signal was detected (Green). The same cells were also probed for fibrillarlin to stain nucleoli. DAPI coloration is used to localize the nuclear compartment. Scale bar 25 μm . Source data are provided as a Source Data file.

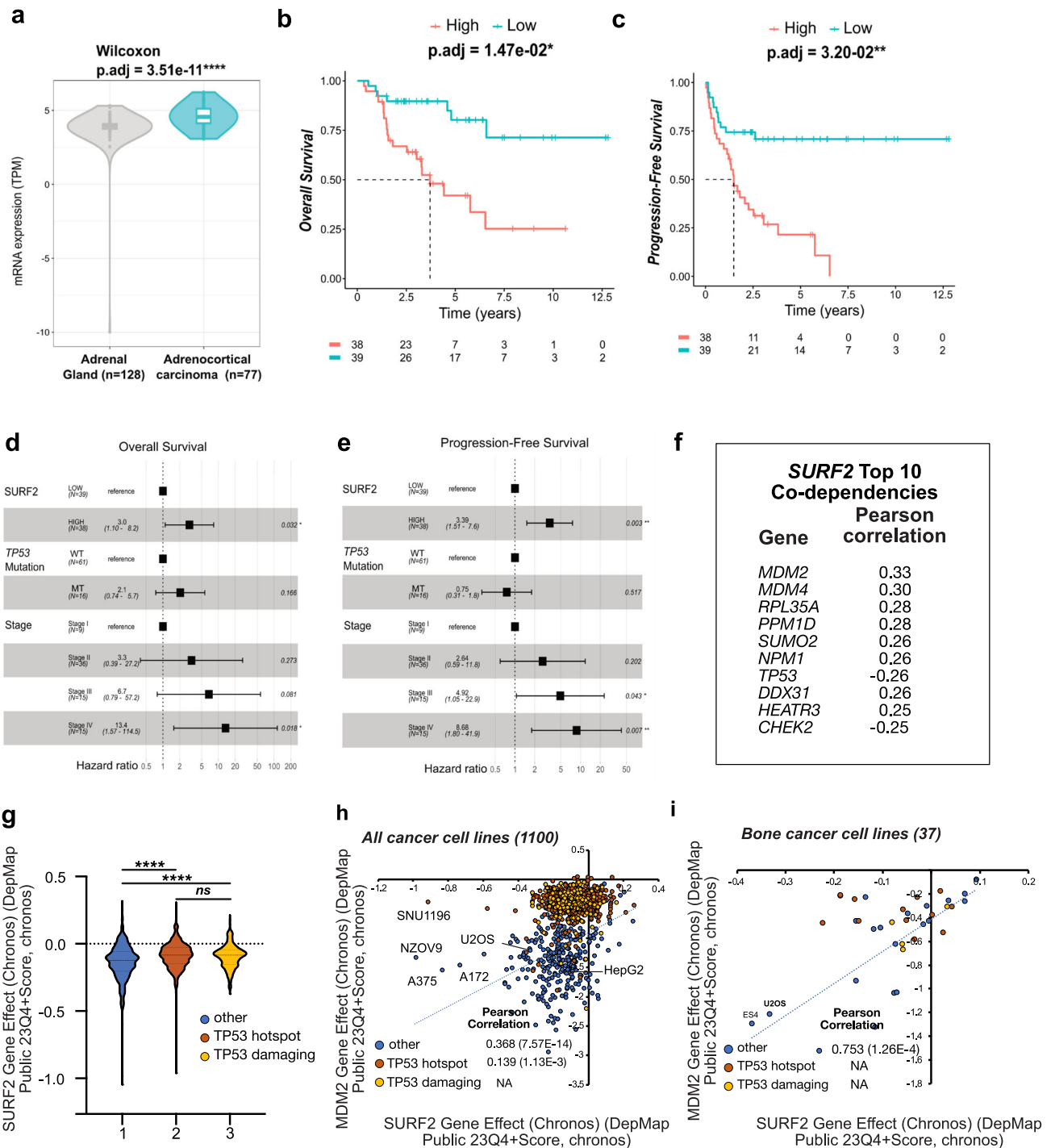
antibodies did not work for immuno-fluorescence experiments in our hands. Therefore, we developed a U2OS cell line expressing a SURF2-eGFP tagged version in the presence of tetracycline. When expressed in the same range as the endogenous one, SURF2-eGFP localized mainly to the nucleoplasm and was also more weakly detected in the nucleolus, supporting the PSE result (Fig. 2e).

To formally exclude the role of SURF2 in ribosome assembly, we assessed whether SURF2 depletion using siRNAs influences ribosome assembly in U2OS cells. We confirmed an 85% reduction in SURF2 protein accumulation by western-blot analysis after 96 h of treatment by two successive transfections with siRNAs (Figs. 3c, d and 4c, d). Our siRNAs strategy using a siRNAs pool was further validated by testing individual siRNAs (Supplementary Fig. S3A, S3B). As a consequence, we kept this pool treatment through the remaining part of this study. After SURF2 depletion, we analyzed the pre-rRNA maturation process by northern blots (Supplementary Fig. S3C, S3D). Data were quantified by Ratio Analysis of Multiple precursors (RAMP), which detects alterations of rRNA maturation by displaying the ratios between one pre-RNA and its immediate processing product^{34,52}. No obvious changes in the accumulation of mature rRNAs, nor of their precursors, were

observed after SURF2 depletion. The combined analysis of three northern blots showed no significant difference in the relative levels of the 32S, 30S, 21S, 12S, or 18S-E precursors (Supplementary Fig. S3D). This absence of pre-rRNA processing defects was confirmed by sucrose gradient analyses, showing no depletion of the small or large ribosomal subunit or other changes (Supplementary Fig. S3E). SURF2 was found in the lighter fractions of the gradient, supporting the association with 5S RNPs but not (pre-) or mature ribosomal particles. The association of RPL5 and RPL11 with ribosomal particles was tested by sucrose gradients and western-blot analysis, compared to RPL17 (Supplementary Fig. S3F, S3G). Their association was unaffected by SURF2 depletion. Altogether, our data support the conclusion that SURF2 does not intervene in ribosome assembly, and interacts only with the free form of 5S RNP particles.

SURF2 is overexpressed in several cancers and is linked to MDM2-p53 pathway

In cancer, NS stress and p53 regulation can participate in both tumor development and drug response. Based on the link between SURF2 and free 5S RNP particles we wanted to test if its expression was affected in



cancer. We performed a PanCancer study, using both the GTex and TCGA resources. First, we compared SURF2 mRNA levels in 29 cancer types relative to their associated healthy tissues (Supplementary Table S4). In 27 of the evaluated cancers, we found an increased level of SURF2 mRNA compared to healthy tissue, indicating that SURF2 is over-expressed in several cancer types. Second, we analyzed the association between SURF2 mRNA expression and overall or progression-free survival across cancers (Table S5). Using TCGA datasets, we found that SURF2 mRNA levels are significantly associated with patient survival in a single cancer type, i.e., adrenocortical carcinoma (Fig. 3a–c and Supplementary Table S5). In this cancer, high levels of SURF2 expression significantly correlate with poor overall survival compared to low expression of SURF2 (25% at 6 years, p_{adj} value=0.01) (Fig. 3b). Interestingly, this difference and trend are conserved in progression-

free survival (p_{adj} = 0.03) (Fig. 3c). To determine whether this association occurs independently of key clinical characteristics, we performed multivariate analysis including SURF2 expression levels, TP53 mutation status and tumor stage as parameters in a Cox regression analysis to compare SURF2 mRNA expression effect association with survival to clinical stages (Fig. 3d, e). It appeared that in adrenocortical carcinomas, both high SURF2 mRNA levels and high tumor stage remained significantly associated with poor survival, in contrast to the presence of TP53 mutation. Thus, SURF2 mRNA levels are an independent marker of poor prognosis in adrenocortical carcinoma.

Considering that SURF2 expression is increased in cancer and that it is able to bind to free 5S RNP particles, we tested whether this increase in SURF2 level was linked to the function of free 5S RNP particles on the regulation of the MDM2-p53 pathway. To this end, we

Fig. 3 | SURF2 is overexpressed in adrenocortical carcinomas and its knock-out negatively affects cancer cells similarly to MDM2. **a** Comparison of *SURF2* mRNA levels in non-tumoral (left panel, gray values) and tumoral tissues (right panel, blue values). Data were extracted from the standardized Xena database to compare healthy adrenal gland tissues ($n = 128$, origin GTEx dataset) and adrenocortical carcinoma tissues ($n = 77$, origin TCGA dataset). Compared to healthy adrenal gland tissues, *SURF2* mRNA levels are higher in adrenocortical carcinoma tissue. ****: $p < 0.0001$ (Wilcoxon Test). Data are presented as a violin plot. It comprises a density plot, the width of which indicates the frequency, and a box plot, where the extreme points reflect the minimum (Q0) and maximum (Q4), the length of the box represents the interquartile range (IQR: percentile Q1 to Q3) and the center represents the median. **b, c** Association between *SURF2* mRNA levels and patient survivals. Using the standardized Xena dataset, associations between *SURF2* mRNA levels (median as cut-off value) and overall survival (**b**) or progression-free survival (**c**) were determined using Kaplan-Meier curves. A significant association was observed between high levels of *SURF2* mRNA levels and poor patient survival. *: $p < 0.05$; **: $p < 0.01$ (Log-rank). **d, e** Association between *SURF2* mRNA levels and patient survivals after adjustment on clinical parameters. Using the standardized Xena dataset, multivariate Cox regression models for overall survival (Low $n = 39$,

High $n = 38$) (**d**) or progression-free survival (**e**) were performed on clinical parameters significantly associated with patient survivals (*i.e.*, *TP53* mutation status and tumor stage, See Supplementary Table S6). High mRNA levels of *SURF2* and stage IV are independent markers of poor survival of patients carrying adrenocortical carcinoma. *: $p < 0.05$; **: $p < 0.01$ (Cox Proportional-Hazards Model, two-sided hypothesis test). Error bars show 95%CI (confidence interval) and square HR (hazard ratio), p -value (0.032 and 0.003 respectively), source data are provided as a Source Data file. **f** Top *SURF2* correlated genes in Project Achilles. The Pearson correlation score on the right indicates the strength of co-dependencies between *SURF2* and the indicated genes. **g** *SURF2* knock-out chronos effect on different cancer cells classified into three groups depending on their *TP53* status: wild-type (blue, $n = 386$), hot-spot mutations (brown, $n = 545$), damaging mutations (yellow, $n = 169$). The data are presented as the mean \pm s.d. Statistical analysis by two-way ANOVA with Turkey's multiple comparisons test. Significant differences are indicated by p -value < 0.0001 (****) (ns = no significance). **h** Classification of more than 1000 cancer cells based on their associated chronos effect of *SURF2* knock-out and *MDM2* knock-out. Pearson correlation between the two chronos effects is indicated depending on *TP53* status. **i** Same as in (**h**) but focusing on bone cancer cell lines. Source data are provided as a Source Data file.

took an unbiased approach by analyzing datasets from the Cancer DependencyMap project (DepMap portal <https://depmap.org/portal>). The DepMap is an ongoing project that systematically assesses the effect of single-gene inactivation on cell proliferation by genome-wide CRISPR screens across a large panel of well-characterized human cancer cell lines p53 (> 1000). The dependency of cancer cells on a gene is indicated by its Chronos score (ProjectAchilles)⁵³. Positive or negative Chronos scores suggest either increased or decreased proliferation, respectively, upon gene KO (a score of -1 indicates the gene as essential in the associated cell line). On average, *SURF2* was indicated as a strongly selective gene that affects proliferation but not as essential (Chronos score around -0.25). Then, we analyzed the effects of *SURF2* knockout on more than 1000 cancer cell lines. As a first analysis, we looked for co-dependency of cancer cells to knockout of other genes as it is often indicative of a role in similar pathways (Figs. 3f and 4f). Interestingly, the top 10 co-dependencies were found with genes involved in the p53 pathway and with *MDM2* in particular, suggesting again a strong relation between *SURF2* and the *MDM2*-p53 pathway. To go further, we compared the Chronos score on cells harboring wild-type *TP53* genes to mutated genes defined as damaging or as hotspot mutation (Fig. 3g). As seen on our violin plot, *SURF2* depletion is more deleterious in cancer cells that express wild-type p53, confirming the strong functional correlation between *SURF2* and p53. Nevertheless, in *TP53* mutant cells, *SURF2* depletion still negatively impacts cancer cells, suggesting that in addition to promoting p53 activation, *SURF2* also induces p53-independent negative effects. *MDM2* is the most strongly co-dependent gene found by DepMap analysis and is required for p53 activation by free 5S RNPs upon nucleolar stress. Therefore, we wanted to test how these genes correlated in different cancers. We thus analyzed the correlation between the knockout effect of *SURF2* and *MDM2* on all cancer cell lines in the dataset or on bone cancer cell lines in which the correlation was stronger (Fig. 3h, i). In this different analysis, we observed a Pearson correlation of 0.368 (p -value 7.57×10^{-14}) and 0.738 (p -value 1.26×10^{-4}) in all cancers or in bone cancers, respectively, for cancer cell lines harboring a wild-type p53. This correlation was strongly reduced or lost in cells harboring *TP53* mutations.

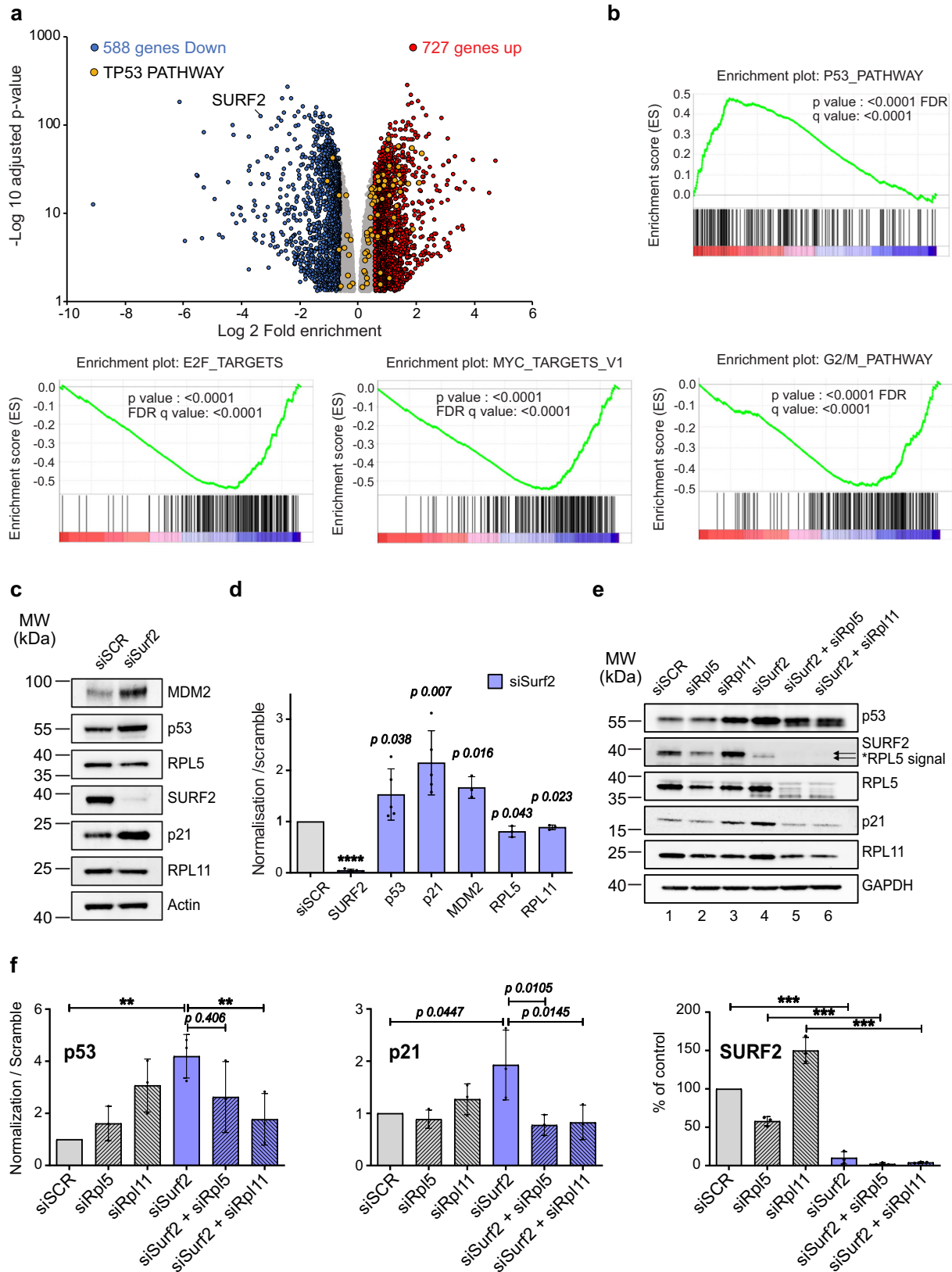
SURF2 depletion promotes p53 activation independent of NS induction

In view of *SURF2*'s role in the regulation of p53 in cancer, its strong connection with *MDM2* highlighted by the DepMap data, and its association with free 5S particles, we wished to initiate the functional characterization of this factor using U2OS cells. To characterize the functions of *SURF2*, we used our siRNAs strategy to perform an RNA-seq

analysis (GSE267134). We analyzed differentially expressed genes (DEGs) from three independent experiments in which U2OS cells were treated either by scrambled (siSCR) or by siRNAs targeting *SURF2*. *SURF2* depletion significantly affected gene expression, with 588 down-regulated genes and 727 up-regulated ones (Fig. 4a and Supplementary Table S7). Gene Set Enrichment Analysis (GSEA) was conducted to identify pathways affected by *SURF2* depletion among all Hallmark's pathways. Interestingly, the most significantly up-regulated pathway was the p53 pathway, whereas the most significantly down-regulated ones were E2F, MYC, and G2/M checkpoint, all supporting a function of *SURF2* in regulating cell proliferation, including cell cycle (Fig. 4a, b and Supplementary Tables S8, S9). Moreover, the data reinforce the functional relationship between *SURF2* and p53 pathways.

Free 5S RNP induces NS response by notably promoting p53 stabilization and expression of its target gene *p21/CDKN1A*, which in turn triggers G1 arrest and/or apoptosis. Our observations on *SURF2* binding to free 5S RNP and its role in p53 regulation could thus indicate that *SURF2* depletion promotes p53 activation by free 5S RNPs. Therefore, using siRNAs and western blots, we investigated by western blots whether *SURF2* depletion promotes p53 activation in the absence of NS exposure by western blots. As a control, we used cells treated with scrambled siRNAs. After *SURF2* depletion alone in U2OS cells, we observed increased protein levels for p53, p21, and *MDM2* compared to control conditions (Fig. 4c, d).

To determine whether the activation of p53 induced by *SURF2* depletion was related to or independent from free 5S RNP function, we repeated *SURF2* depletion in the absence of RPL5 or RPL11, conditions known to abolish p53 stabilization²² (Fig. 4e, f). Following the treatments with various combinations of siRNAs, the accumulation of NS-related proteins involved in p53 regulation was examined by western blot (Fig. 4e, f). As previously reported, depletion of either RPL5 or RPL11 reduced the level of the other²⁴ (Fig. 4e, lanes 5 and 6 compared to 2 and 3, Supplementary Fig. S4A). This was also found for *SURF2*; depletion of RPL5, RPL11, or *SURF2* proteins affects the stability of the two other members of this group, strongly supporting direct interactions (Fig. 4e, f and Supplementary Fig. S4A). After U2OS cells treatment with siRPL5 or siRPL11, mild accumulations of p53 and p21 were observed that could reflect a slight NS response that would occur before protein depletion really affects free 5S RNPs accumulation (Fig. 4e, f). A greater accumulation of p53 was observed after RPL11 depletion but without correlated p21 induction. This confirms previous results showing that although RPL5 and RPL11 depletion hinders ribosome assembly, their depletion impedes p53 and p21 accumulation by free 5S particles^{14,22}. In this set of experiments, we were able to confirm by western blots that *SURF2* depletion



significantly promotes both p53 and p21 accumulation (Fig. 4e, f). However, when SURF2 is co-depleted with RPL5 or with RPL11, we could no longer observe any p21 accumulation, while p53 stabilization was reduced by 25% or 50%, respectively (Fig. 4e, lanes 5 and 6 and 4 F). This result indicates that the SURF2 depletion effect on p53 activation is mediated by free 5S particles, independently of NS induction.

SURF2 depletion increases MDM2 binding to free 5S RNP particles

SURF2 expression is increased in numerous cancers (Supplementary Table S4), and our DepMap analysis indicates a potential functional co-dependency between SURF2 and MDM2. Moreover, we showed that in U2OS cells, SURF2 depletion promotes p53 activation through free 5S

Fig. 4 | SURF2 depletion up-regulates the p53 pathway. RNA-seq analyses of SURF2 depletion. U2OS cells were treated by scramble siRNAs or by siRNAs against SURF2 for 96 h. mRNA expression levels were compared between the two conditions, and experiments were repeated ($n = 3$). **a** Volcano plot showing significantly differentially expressed genes. Using DESeq2, a comparison of gene expression between the customer-defined groups of samples was performed. The Wald test was used to generate p -values and \log_2 fold changes. Genes with an adjusted p -value < 0.05 and absolute \log_2 fold change > 1 were called differentially expressed genes indicated: up-regulated genes (red) and down-regulated (blue) or unaffected (gray). Genes from the TP53 pathway are highlighted yellow. **b** Gene set enrichment analysis (GSEA) in SURF2 depleted genes or in the control condition (siSCR). ES; enrichment score. GSEA P -values were derived from permutation testing and corrected for multiple testing using the False Discovery Rate (FDR) method. Enrichment score (ES) and FDR value were applied to sort SURF2 depleted and control cells genes-enriched after gene set permutations were performed 1000 times for the analysis. Gene Network Analysis was based on DEGs (\log_2 foldchange > 1). **c** Western-blot analyses showing the accumulation of different proteins in 20 μ g of

cellular extracts produced from U2OS cells treated with scrambled siRNAs (siSCR) or with siRNAs directed against SURF2 (siSurf2). **d** Quantification of signals obtained by western-blot analysis and normalized to actin signals in each condition (c) from independent biological replicates (p53, $n = 5$; SURF2, $n = 5$; p21 $n = 5$; MDM2, $n = 3$; RPL5, $n = 3$; RPL11, $n = 3$). Two-tailed t -test analysis was used for statistics. Data are presented as mean values \pm SD. Significant differences are indicated by stars (p -value $\leq 0.05^*$; $\leq 0.01^{**}$; $\leq 0.001^{***}$ and $\leq 0.0001^{****}$) or with the precise p -value on the graph (p). **e** Co-depletion experiment. Western-blot analyses showing the accumulation of different proteins in 20 μ g of cellular extracts issued from U2OS cells treated with a combination of different siRNAs: scrambled (siSCR); RPL5 (siRPL5); RPL11 (siRPL11) or SURF2 (siSurf2). **f** Quantification of signals obtained by western-blot analysis and normalized to GAPDH signals in each condition (h) ($n = 3$). Data are presented as mean values \pm SD. A one-way ANOVA test was used for statistics. Significant differences are indicated by stars (p -value $\leq 0.05^*$; $\leq 0.01^{**}$ and $\leq 0.001^{***}$) or with the precise p -value on the graph (p). Source data are provided as a Source Data file.

RNPs, even in the absence of nucleolar stress. As previously described, free 5S RNP promotes p53 activation through sequestration of MDM2, its primary negative regulator. To decipher how SURF2 might regulate p53 through free 5S RNPs function, we investigated whether and how SURF2 was related to MDM2. While studying SURF2 interactome, we could not find any interaction of SURF2 with MDM2 nor with p53 (Fig. 2a and Supplementary Table S3). This data indicates that the regulation of free 5S RNP function might not occur through a direct interaction between SURF2 and MDM2. We thus tested how SURF2 might affect the binding of free 5S RNP particles to MDM2. First, we performed IPs of free 5S RNP particles in the presence or absence of SURF2, using RPL5-Flag as bait. Since the interaction between free 5S RNP and MDM2 is enhanced after NS, we performed these IPs before or after NS exposure by treating U2OS cells with low dose of actinomycin D (ACTD, as for Fig. 1). We used a U2OS cell line that does not express RPL5-Flag as a control (Fig. 5a). As expected, only a mild but specific retention of MDM2 and p53 is observed in cells expressing RPL5-Flag under normal conditions. Importantly, no interaction between RPL5-Flag and p21 was identified, confirming that p21 accumulation only reflects p53 transcriptional activity. Under the same conditions, depletion of SURF2 specifically increased interactions of both MDM2 and p53 with RPL5-Flag (Fig. 5a, b), suggesting that SURF2 regulates the binding of MDM2 to free 5S RNP particles.

SURF2 depletion increases cells sensitivity to NS

In the same set of experiments, Following NS induction by actinomycin D, interactions of both MDM2 and p53 with RPL5-Flag were also increased (Fig. 5a, b). An additional and statistically significant increase of p53 retention with RPL5-Flag is observed when cells are both exposed to NS and depleted of SURF2 (Fig. 5a, b). A similar trend was also observed for MDM2, but the variability of signal quantification between experiments was too high to reach statistical significance. These data indicate that SURF2 depletion promotes both MDM2 and p53 binding to free 5S RNP particles under normal conditions or upon nucleolar stress.

To test whether SURF2 depletion modulates free 5S RNP function in NS response, we reanalyzed the levels of p53, MDM2, and p21 in our previous IPs (Fig. 5a). This showed that p53, p21, and MDM2 were all stabilized both after NS exposure (ACTD) or following SURF2 depletion. Notably, depleting SURF2 in cells exposed to actinomycin D promoted a statistically significant increase in the accumulation of p53 and p21 compared to each condition independently (Fig. 5c). To confirm that SURF2 depletion increases the response to NS, we analyzed the effect on cell cycle progression by flow-cytometry analysis (Fig. 5d). As expected, exposure of cells to actinomycin D induced an accumulation of cells in G1 phase, reflecting cell-cycle arrest. This arrest was also observed following SURF2 depletion alone (Fig. 5d and

Supplementary Fig. S4B). Interestingly, inducing NS in cells depleted of SURF2 promoted an even stronger and more statistically significant G1 arrest (Fig. 5d). We also performed cell proliferation assays on U2OS cells, either depleted of SURF2 with siRNAs, exposed to Actinomycin D or receiving both treatments (Fig. 5e, f). Cell proliferation was assessed in triplicate, using crystal violet staining, at time points up to 36 h. Treatment with anti-SURF2 siRNAs or actinomycin D reduced cell proliferation compared to scramble siRNAs (siSCR). The combination of both treatments had the strongest effect on cell proliferation, and was accompanied by a loss of cellular material between 24 and 36 h of treatment, suggesting a potential apoptosis induction (Fig. 5f). To test this possibility, we used higher concentrations of actinomycin D that will promote more apoptosis, and then test for the effect of SURF2 depletion on apoptosis induction using annexin V labeling using flow cytometry (Fig. 5g). In these assays, actinomycin D or SURF2 depletion by siRNAs induces some apoptosis compared to control experiments (10% and 8% of dead cells, respectively). However, the two treatments together significantly increase apoptosis (20%). We propose that the combination of both treatments promotes apoptosis, in addition to slowing proliferation. To test if this effect of SURF2 depletion on drug sensitivity was only observed with actinomycin D, we also tested other drugs known to induce nucleolar stress, namely 5-FU and BMH-21 (Supplementary Fig. S4B–S4D). There again, we were able to observe an increased sensitivity to ribosome synthesis inhibition, with more G1 arrest and an increase in apoptosis in cells treated both with the drugs and siRNAs targeted towards SURF2 compared to control cells or cells receiving individual treatments (Supplementary Fig. S4B–S4D).

Then, to assess if the negative effect of SURF2 depletion on cell cycle progression was linked to MDM2/p53 pathways, we performed the same analyses in cells either depleted of p53 (siP53) or mutated for this gene (HCT116, TP53^{+/+} compared to HCT116, TP53^{-/-}) (Supplementary Fig S4E, F). In both cases, G1 arrest was significantly reduced, and we could observe more cells in the S phase, strongly supporting the role of p53 in SURF2 depletion-mediated cell cycle defects. However, the absence of p53 does not fully compensate for SURF2 depletion effects on the cell cycle, with some G1 arrest still visible, suggesting additional p53-independent effects of SURF2 depletion on cell cycle progression (Supplementary Fig. S4E, F).

Although our DepMap analysis supports that SURF2 depletion could similarly affect multiple cells by mainly playing on MDM2/p53 pathways, we wanted to test if our observations in U2OS cells upon SURF2 depletion on p53 regulation were also true in other cell lines. Thus, we repeated these experiments using other cancer cell lines; Hepatocellular carcinoma (HCC) HepG2 cell line carrying a wild-type TP53 gene and melanoma A375 cell line, the latter one being reported by DepMap analysis as very sensitive to SURF2 depletion. In HCC cells, SURF2 depletion promoted p53

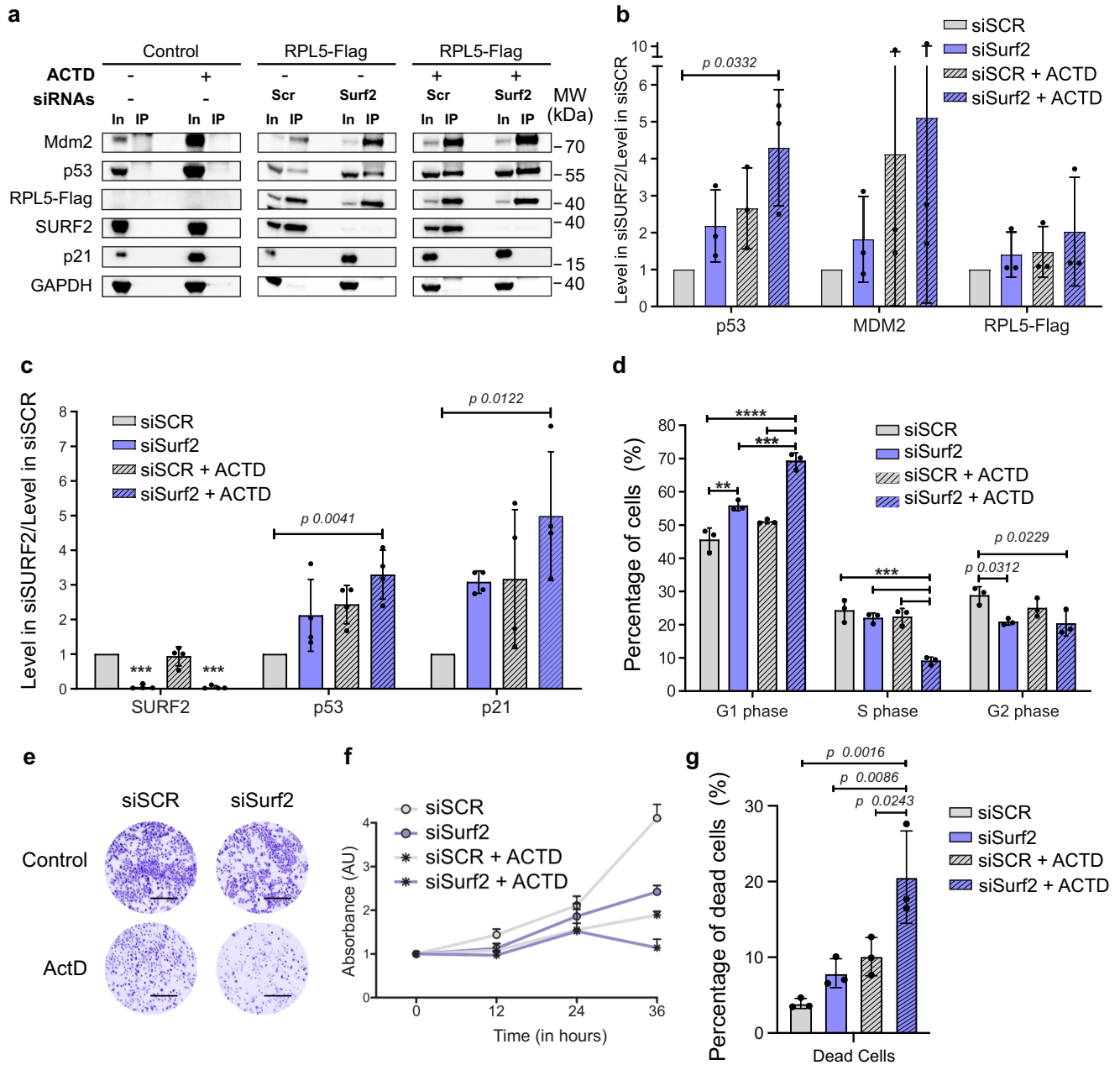


Fig. 5 | SURF2 depletion increases free 5S binding to MDM2 and increases cell sensitivity to nucleolar stress. a Detection of proteins associated with RPL5-Flag. Cell extracts produced from U2OS cells overexpressing RPL5-FLAG or not (control) and differentially treated by actinomycin D addition for 24 h (at 10 ng/mL) or not (ACTD + or -) and transfected with scrambled siRNAs (siSCR) or directed against SURF2 (siSurf2) were used to perform immuno-precipitation on beads coated with anti-flag. 10% of the inputs were loaded (In) aside IPs (IP) on a gel to perform western blots using antibodies directed against the indicated proteins to analyze the co-purification efficiency of the different factors. **b** Quantification of the co-purification efficiency with RPL5-Flag observed (a) for the indicated proteins ($n = 3$). Results are represented as a comparison of the enrichments observed in cells treated with siRNAs directed against SURF2 (siSurf2) normalized to the ones observed in cells treated with scrambled siRNAs (siSCR). Two-tailed t-test analysis was used for statistics. Data are presented as mean values \pm SD. Significant differences are indicated by stars (p -value $\leq 0.05^*$; $\leq 0.01^{**}$; $\leq 0.001^{***}$ and $\leq 0.0001^{****}$) or with the precise p -value on the graph (p). **c** Quantification of the signals corresponding to the indicated proteins in the different inputs of western-blots analyses (a) from independent experiments $n = 4$ (original data are provided in the source data file). Two-tailed t test analysis was used for statistics. Data are presented as mean values \pm SD. Significant differences are indicated by stars (p -value $\leq 0.05^*$; $\leq 0.01^{**}$; $\leq 0.001^{***}$ and $\leq 0.0001^{****}$) or with the precise p -value

on the graph (p). **d** DNA content analysis of U2OS cells treated as indicated (siSCR: scrambled siRNAs; siSurf2: siRNAs against SURF2; ACTD: actinomycin D at 10 ng/mL for 24 h) by FACS. Quantification of U2OS cell repartition in the different phases of the cell cycle following different treatments ($n = 3$). Data are presented as mean values \pm SD. One-way Anova Test was used for statistics. Significant differences are indicated by stars (p -value $\leq 0.05^*$; $\leq 0.01^{**}$; $\leq 0.001^{***}$ and $\leq 0.0001^{****}$) or with the precise p -value on the graph (p). **e, f** Proliferation analysis of differentially treated U2OS cells. Cells are treated as indicated (siSCR: scrambled siRNAs; siSurf2: siRNAs against SURF2; ACTD: actinomycin D at 10 ng/mL for 24 h). **e** Cells are plated on 6 well plate after being transfected with the indicated siRNAs, 24 h before being analyzed, cells were treated with actinomycin D (10 ng/mL) or H2O. Cells were stained with crystal violet to take a picture ($n = 3$) scale bar (0.5 mm). **f** Fixed crystal violet was resolubilized and quantified by absorbance for each condition after different time exposure to treatments ($n = 3$). **g** Cell apoptosis assays with an annexin-V-FITC and propidium iodide of differentially treated U2OS cells. Both apoptosis and necrosis are regrouped as dead cells ($n = 3$). Data are presented as mean values \pm SD. The One-way ANOVA test was used for statistics. Significant differences are indicated by stars (p -value $\leq 0.05^*$; $\leq 0.01^{**}$; $\leq 0.001^{***}$ and $\leq 0.0001^{****}$) or with the precise p -value on the graph (p). Source data are provided as a Source Data file.

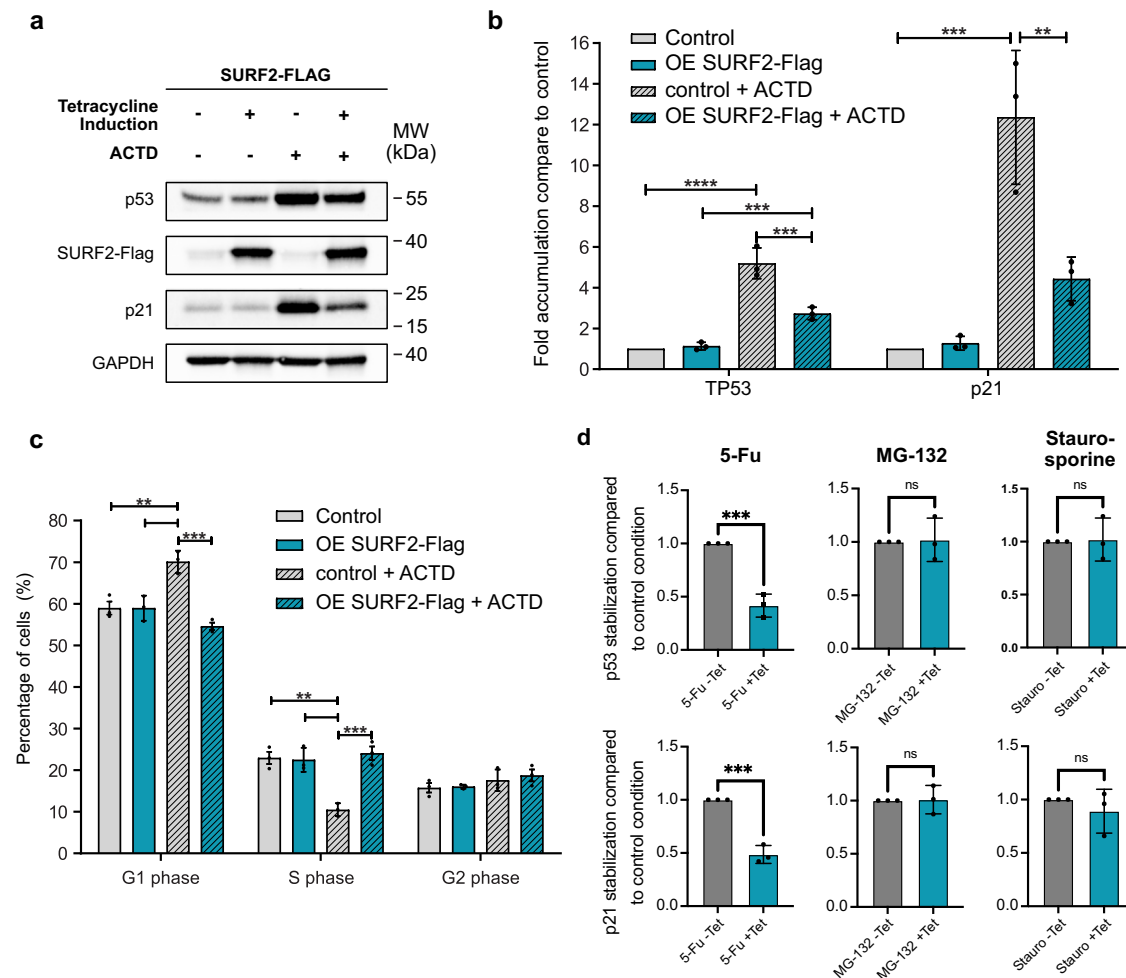


Fig. 6 | SURF2 overexpression impedes p53 activation and cell cycle arrest following nucleolar stress. **a** Western-blot analysis showing the accumulation of different proteins, in 20 μ g of cellular extracts produced from control U2OS cells or from U2OS cells that overexpress SURF2-Flag after Tetracycline induction (1 μ g/ml) from their T-Rex locus for 24 h. Cells were also treated differentially with or without the addition of actinomycin D (10 mg/ml) for the same period ($n = 3$). **b** Quantification of the signals observed in an independent experiment (A) ($n = 3$). Data are presented as mean values \pm SD. One-way ANOVA tests were used for statistics. Significant differences are indicated by stars (p -value ≤ 0.05 ; $\leq 0.01^{**}$ and $\leq 0.001^{***}$). Source data are provided as a Source Data file. **c** DNA content analysis of U2OS cells treated as indicated (Ctrl: U2OS control cells; OE SURF2-Flag: U2OS cells that overexpress SURF2-Flag; ACTD: Treated with actinomycin D) by FACS. Quantification of different U2OS cell repartition in the different phases of the

cell cycle following different treatments is represented as histograms ($n = 3$). Data are presented as mean values \pm SD. One-way ANOVA tests were used for statistics. Significant differences are indicated by stars (p -value ≤ 0.05 ; $\leq 0.01^{**}$ and $\leq 0.001^{***}$). Source data are provided as a Source Data file. **d** Comparison of p53 and p21 stabilization, assessed by western blots, following drugs treatment (5-Fu: 50 μ M; MG-132: 10 μ M; staurosporine: 25 nM for 24 h) in U2OS control cells (uninduced) or in cells overexpressing SURF2-Flag (Tetracycline 1 mg/ml). P53 and p21 signals were normalized to 1 in the control experiment, and relative stabilization in cell overexpressing SURF2-Flag was quantified from three independent biological replicates ($n = 3$). Data are presented as mean values \pm SD. Two-tailed paired T test was used for statistics. Significant differences are indicated by stars (p -value ≤ 0.05 ; $\leq 0.01^{**}$ and $\leq 0.001^{***}$). Source data are provided as a Source Data file.

activation and strongly increased cell sensitivity to actinomycin D (Supplementary Fig. S5A, S5B). The combination of a low dose of actinomycin D treatment and SURF2 depletion further decreased cell proliferation (Supplementary Fig. S5B). In A375 cells, we could not observe a strong p53 stabilization upon SURF2 depletion. However, we could observe a strong p21 accumulation (Supplementary Fig. S5C). The combination of the low dose of actinomycin D treatment and SURF2 depletion further increased this p21 stabilization (Supplementary Fig. S5C).

SURF2 overexpression impedes p53 activation following NS

As SURF2 depletion increases cell response to NS, its overexpression could inversely inhibit cell response to NS. To test this hypothesis, we developed a U2OS Flip-In T-rax cell line with a tetracycline-induced overexpression of SURF2-Flag. To avoid misinterpretation due to side effects of SURF2 overexpression, we verified that this induction did not

alter ribosome assembly (Supplementary Fig. S6A and S6B). We then compared by western-blot analysis the level of p53 and p21 in control cells treated or not with actinomycin D, with or without overexpression of SURF2-flag for 24 h (Fig. 6a). Quantification of these signals confirmed that cell exposure to actinomycin D promotes p53 stabilization and activity, as reflected by p21 increased levels (Fig. 6b). In stark contrast, cells overexpressing SURF2 showed only a mild increase in p53 and p21 levels (Fig. 6a, b). These data indicate that overexpression of SURF2-Flag impedes p53 activation by free 5S RNP. To confirm this observation, we performed cell cycle analysis by flow cytometry using the same cells and treatments, and quantified the percentage of cells in each phase (Fig. 6c). Exposure to actinomycin D promotes G1 arrest in untreated cells, but overexpression of SURF2-Flag completely blocks this response (Fig. 6c). This result indicates that overexpression of SURF2 inhibits NS response in U2OS cells in this time frame. To test if the compensatory effect of SURF2

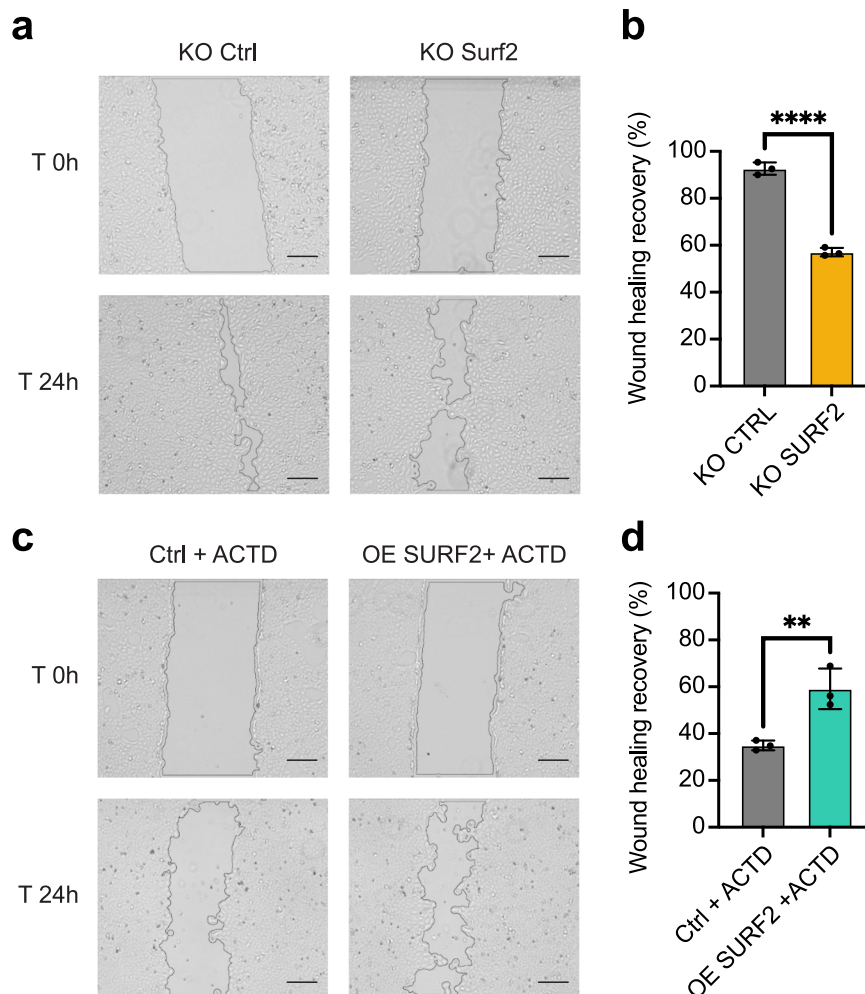


Fig. 7 | SURF2 expression level affect U2OS phenotypic traits. Analysis of U2OS KO SURF2 or U2OS overexpressing SURF2-Flag cell migration by wound healing assay. **a, c** Images were taken with Cell Imaging EVOS (Gx40) at 0 h and 24 h ($n = 3$) (scale bar = 0.1 mm). **b, d** Quantification of wound healing by measuring the percentage of persistent scar area after 24 h from three independent biological

replicates ($n = 3$). Use of an unpaired two-tailed t test for statistical tests Data are presented as mean values \pm SD, and significant differences are indicated by stars as follows p -value $< 0.05^*$; 0.01^{**} 0.001^{***} and 0.0001^{****}) or with the precise p -value on the graph (p). Source data are provided as a Source Data file.

over-expression on p53 stabilization upon drug treatment, was related to its role in nucleolar stress regulation, or was related to a more general p53 regulation pathway, we repeated these experiments using either another drug (5-FU) that induced nucleolar stress and requires the free 5S RNPs, or drugs that regulate p53, independently of nucleolar stress: the proteasome inhibitor MG-132, or the broad-spectrum protein kinase inhibitor staurosporine¹⁴. We then compared the effect of SURF2 overexpression on both p53 and p21 stabilization promoted by these different drugs (Fig. 6d). The quantification of the p53 and p21 levels upon drug treatments, from three independent experiments, clearly shows that SURF2 overexpression compensates for p53 and p21 levels when cells are treated by 5-FU, as for actinomycin D. In contrast, SURF2 overexpression is not able to compensate for p53 nor p21 stabilization induced by MG-132 or staurosporine exposure. These data, strongly argue for a specific role of SURF2 overexpression in impairing both p53 and p21 stabilization upon drugs that induce nucleolar stress.

SURF2 expression levels affect U2OS capacity to migrate

Our precedent data on SURF2 depletion or sur-expression that modulate NS stress sensitivity, clearly place SURF2 as a key factor able to regulate nucleolar stress response. Furthermore, we have demonstrated that SURF2 is overexpressed in most cancers. In order to test

how SURF2 expression could affect phenotypic traits of cancer cells, we developed knock-out SURF2 cell lines using CRISPR technology. To obtain these cell lines clearly demonstrates that this factor is not essential in U2OS, confirming DepMap data. We then compared the capacity of control and KO SURF2 cells to migrate in a wound healing assay (Fig. 7a, b). Our results demonstrate that deletion of SURF2 impedes cells capacity to migrate. We also used the same approach to assess the effect of SURF2 overexpression on wound healing assays (Fig. 7c, d). During these experiments, we could observe that, conversely to its deletion, overexpressing SURF2 increases cancer cells capacity to migrate upon nucleolar stress induction (Actinomycin D treatment).

Over-expressed SURF2 impedes MDM2 binding to 5S RNP in vivo

In light of our previous results, to decipher the molecular function of SURF2, we wondered whether SURF2 regulates MDM2 binding to free 5S RNP particles. We assessed free 5S RNP particle binding by recovery of RPL5, RPL11, and 5S rRNA on beads coupled with either anti-MDM2 or anti-SURF2 antibodies and with beads devoid of antibodies as control (Fig. 8a-c). Free 5S RNP association was tested following exposure to NS, in control cells or cells overexpressing SURF2-Flag from the U2OS-T-rex locus. In control cells (not overexpressing SURF2-Flag), we clearly observed specific retention of RPL5, RPL11, and 5S

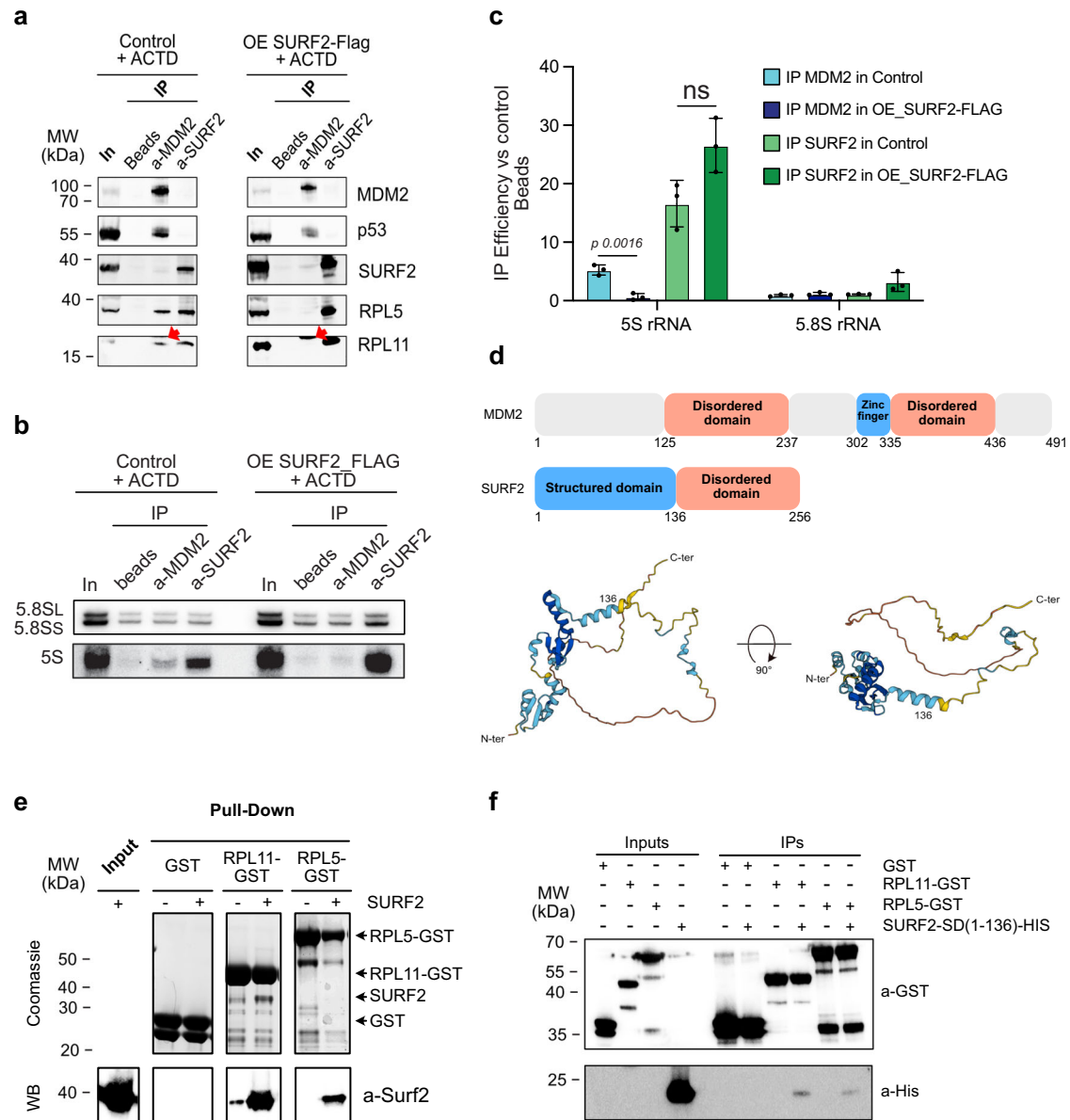


Fig. 8 | SURF2 is able to directly interact with both RPL5 and RPL11 and competes for their binding with MDM2 in vivo. **a** Extracts from U2OS cells that overexpress SURF2 (OE SURF2-Flag) or not (control) and treated by actinomycin D (ACTD) are used to perform IPs using beads only, beads coupled to anti-SURF2 or beads coupled to anti-MDM2. After washes, the remaining proteins are resuspended in loading dye and analyzed by western blots using the indicated antibodies. Red arrows indicate unspecific bands (IgG) ($n = 2$). **b** Same as in (a) but using northern blot to test for RNA binding. Probes against 5S and 5.8S were used ($n = 3$). **c** Quantification of northern-blot signals to test for specific enrichment of RNA species ($n = 3$). Use of an unpaired two-tailed t test for statistical tests. Data are presented as mean values \pm SD, and significant differences are indicated by stars as follows p -value < 0.05 *; 0.01 ** 0.001 *** and 0.0001 ****) or with the precise p -value

on the graph (p). **d** Secondary structure of SURF2 and MDM2 proteins. Functional domains are indicated. SURF2 3D structure modelization by Alphafold software is represented. **e** GST-pull-down assays. Extracts of BL21 that overexpress recombinant SURF2-HIS were mixed with extracts that overexpress either GST alone, GST-RPL5, or GST-RPL11. Proteins specifically retained on glutathione-sepharose beads were analyzed both by Coomassie staining and western-blot analysis (WB). 10% of the extracts were used for inputs ($n = 2$). **f** Same experiments as in (e) but replacing extract with SURF2-HIS by extracts that overexpress structural domain of SURF2 (SURF2-SD-HIS) as prey. Proteins specifically retained on glutathione-sepharose beads were analyzed both by western blots with indicated antibodies ($n = 2$). Source data are provided as a Source Data file.

rRNA with anti-MDM2 or anti-SURF2 antibodies. This demonstrates that free 5S RNP particles can interact with these two factors. Notably, SURF2 was not retained by anti-MDM2, nor MDM2 by anti-SURF2, consistent with our interactome analysis (Fig. 2a, b). In cells overexpressing SURF2-Flag, RPL5, RPL11, and 5S rRNA were enriched in total cell extracts (see inputs Fig. 8a), potentially reflecting their stabilization in a complex formed by SURF2-RPL5-RPL11-5S rRNA. Despite this, we repeatedly ($n = 4$) failed to detect any signal for RPL5, RPL11, or 5S rRNA in the IPs using anti-MDM2 coupled beads in cells

overexpressing SURF2-Flag (Fig. 8a–c). We conclude from these experiments that over-expression of SURF2 impedes free 5S RNP binding to MDM2 following treatment with actinomycin D.

SURF2 interacts directly with RPL5 and RPL11 in vitro

Following NS, MDM2 binds to free 5S particles mainly through direct interaction with RPL11, mediated by its zinc-finger domain^{36,42}. A mutation in this domain (MDM2C305F) fully abolishes its interaction with free 5S particles⁵³. The previous results suggested that SURF2 and

MDM2 association with free 5S RNP might be mutually exclusive. To test this hypothesis, we performed pull-downs using recombinant RPL5-GST, RPL11-GST, or GST alone purified from *E. coli* (Fig. 8e). The purified proteins were incubated with the same amount of recombinant SURF2-HIS and performed GST pull-down assays (Fig. 8e). We observed weak but specific retention of recombinant SURF2 on beads coated with RPL5-GST or RPL11-GST but not with GST alone, both by Coomassie staining and western-blot. Comparison of SURF2-HIS signals indicated that RPL11-GST retains more SURF2 than does RPL5-GST, although association was seen for both proteins (Fig. 8e). Like MDM2, SURF2 contains an intrinsically disordered domain (Fig. 8d). To decipher by which domain SURF2 interacts with RPL5 and/or RPL11 generated truncated SURF2₁₋₁₃₆-GST, corresponding to its structured domain (hereafter termed SURF2-SD) (Fig. 8d, f). Due to intrinsic instability, we could not test the interaction of SURF2-disordered domains using similar experiments. SURF2-SD was bound by both RPL11-GST and RPL5-GST, with greater binding to RPL11 (Fig. 8f). Preferential binding to RPL11, by both the structured domain of SURF2 and the disordered domain of MDM2, suggests a mechanism for their competitive binding to free 5S RNPs.

Discussion

Free 5S RNP particles are key in the response to nucleolar stress, a cellular mechanism that is instrumental to cancer treatment by chemotherapeutic drugs. Thus, promoting the extra-ribosomal activity of free 5S RNPs in wild-type TP53 cancers may improve the p53-dependent anticancer effects of therapeutic agents such as chemotherapy used in most poor-prognosis cancers. In order to understand how the function of these particles could be regulated at basal level and under nucleolar stress conditions, we undertook the characterization of these particles in U2OS cells, a cell line known to be very sensitive to NS and in which the correlation between SURF2 and p53 pathway is strong (Fig. 3i). We retrieved well-known partners of free 5S RNP particles, such as SSB/La and MDM2 (Fig. 1a). SSB/La, a chaperone of 5S rRNA, binds this RNA just after its transcription³⁸. The specific enrichment of SSB/La protein with RPL5-Flag suggests that during 5S particle biogenesis, there is a transient intermediate containing both La and RPL5. Other known partners, such as HEATR3 and BXDC1/RPF2, were also found associated with RPL5-Flag but with a statistic significance below our threshold ($-\log_{10}(p\text{-value}) < 1$) of 0.974 and 0.929 reciprocally (Supplementary Table S1). In addition, we identified the tumor suppressor p53 as a partner of free 5S RNP particles and were able to show that this interaction is mediated through MDM2. So, how free 5S RNP particles fully inhibit MDM2 catalytic activity and promote p53 function remains elusive and will need further examination. Interestingly, the fact that we can purify free 5S RNP particles even in the absence of stress demonstrates that a portion of these particles are not incorporated into ribosomes even in a proliferative cell state. This overproduction of free 5S RNP particles observed in our experiments, even in the absence of stress, may find its origin in the genomic and transcriptional independence of 5S rRNA compared to other rRNAs, which most likely fails to warrant a fully equilibrated production of rRNAs. Interestingly, 5S rRNA both genomic and transcriptional independence of 5S rRNA has been reinforced during evolution, going from an extra-copy of 5S rDNA in some bacteria, such as *E. coli*, to transcriptional independence in yeast *S. cerevisiae* and segregation of rDNA and 5S genes on different chromosomes in Humans. Therefore, differential production of 5S rRNA compared to the other rRNAs seems to give an advantage to the cells, but how this occurs remains an open question.

In addition to these factors, we found a potential partner and preceding uncharacterized factor, SURF2 (Fig. 1A). SURF2 is a member of the surfeit genomic locus that contains 6 genes, all involved in promoting cell proliferation. Furthermore, it shares a bidirectional promoter with SURF1 that is positively regulated by the oncogene

c-Myc, which highly supports cell proliferation in numerous cancer^{46,54}. In this line, our PanCancer study supports an overexpression of SURF2 in cancers, as it has been found overexpressed in 93% of the analyzed cancers compared to healthy tissues (Fig. 3a and Supplementary Table S4). In the course of its characterization, we were able to show that this mainly nucleoplasmic factor is not directly involved in pre-ribosomes processing and only interacts with 5S RNP particles independently of ribosomes in their free state (Fig. 2). Moreover, using the DepMap portal, we were able to find that SURF2 knock-out negatively affects several cancer cell lines, in both a p53 dependent and independent manner, although the deleterious effect is stronger in cell harboring TP53 WT. This negative effect on cancer cell proliferation strongly positively correlates with MDM2 knock-out, suggesting that most SURF2 effects are associated with MDM2 regulation (Fig. 3f, h, and i). This strong relation between SURF2 and MDM2-P53 pathway was then confirmed by RNA-seq analysis that showed that in the absence of SURF2, more than 1000 genes were deregulated, the p53 pathway being the most up-regulated one (Fig. 4a, b). This analysis suggests that SURF2 depletion promotes p53 stabilization. Interestingly, other regulatory pathways that are inhibited upon SURF2 depletion, such as c-myc and E2F, are also known to be inhibited in answer to nucleolar stress, notably by RPL11⁵⁵. This observation suggests that SURF2 depletion could also play a role in p53-independent nucleolar stress response by freeing RPL11 or the whole free 5S RNPs to assume other extra-ribosomal and p53-independent regulations. We then showed, using different cancer cell lines (U2OS, HepG2, and A375), that in the absence of SURF2, cells accumulate p53 and p21 in a free 5S RNP-dependent manner, with or without inducing nucleolar stress (Fig. 4c, e, f and Supplementary Fig. S5A, S5B and S5C).

In response to nucleolar stress induced by actinomycin D, cells depleted of SURF2 showed a greater accumulation of p53 and p21 and a stronger arrest in the G1 cell cycle with associated cell death compared to control cells (Fig. 5d–g). This was also observed for other drugs (5-FU, BMH-21, and staurosporine) (Supplementary Fig. S5B, S5C, and S5D). Of note, the G1 arrest observed upon SURF2 depletion is not fully compensated by p53 depletion or mutation, suggesting again that SURF2 could also play a p53-independent regulation of the cell cycle. Interestingly, among the different pathways down-regulated in our RNA-seq analysis, we found the c-myc one, which is known to be negatively regulated upon nucleolar stress by RPL11⁵⁶. Indeed, many p53-independent mechanisms are activated upon nucleolar stress, with some relying on free 5S RNPs⁵⁷. This greater cell sensitivity to nucleolar stress in the absence of SURF2 is associated with an increased ratio of free 5S RNP particles associated with MDM2 and p53 (Fig. 5a, b). Reciprocally, an over-expression of SURF2 impedes p53 activation and cell cycle arrest, which are normally induced by NS, and abolishes the interaction between free 5S RNP particles and MDM2 (Figs. 6a, b, 8a, b). Without NS, overexpression of SURF2 does not affect basal p53 nor p21 levels, this can be explained by two non-mutually exclusive hypotheses: In the absence of NS, all free 5S RNPs are already bound by SURF2, therefore increasing SURF2 expression does not affect the amount of free 5S that can interact with MDM2; or in these conditions p53 and p21 are already at their lowest and cannot be further reduced. Interestingly, this over-expression of SURF2 only compensates for p53 and p21 stabilization induced by nucleolar stress-promoting drugs, supporting a strong functional specificity of SURF2 in relation to free 5S RNPs and nucleolar stress response. Our results further show that the interaction of SURF2 or MDM2 with free 5S particles is mutually exclusive *in cellulo* and that SURF2 mainly interacts with free 5S particles through binding to RPL11, which involves SURF2's structural domain (Fig. 8).

All these observations support a functional model presented in Fig. 9. In normal conditions (ie, without nucleolar stress), SURF2 acts as a buffer for free 5S RNP particles that could accumulate compared to other ribosomal components (Fig. 9a). In response to NS, due to chemotherapeutic drugs for example, a greater portion of free 5S RNP

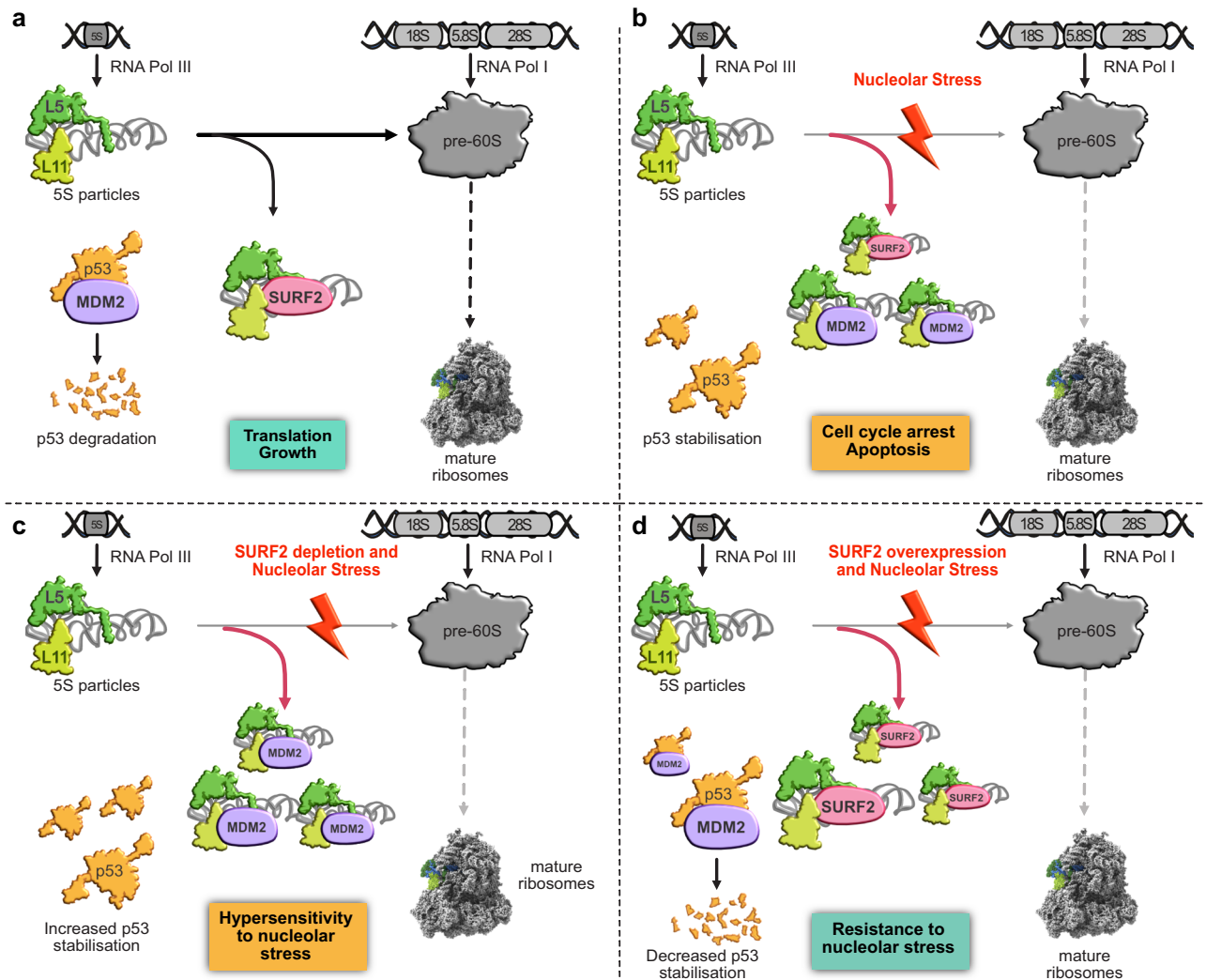


Fig. 9 | Model of SURF2 function in free 5S RNP regulation. Schematic representation of free 5S regulation by SURF2 in different conditions. **a** In normal cells, both 5S and 47S rDNAs are transcribed by RNA polymerase III and I, respectively. Ribosome synthesis is producing pre-60S ribosomes and 5S particles constituted by the association of RPL5 and RPL11 to 5S rRNA are incorporated into these large pre-ribosomes. The remaining overproduced free 5S are bound by SURF2 to avoid MDM2-Free 5S interaction, which would induce p53 stabilization and cell cycle arrest. At the same time, p53 is constantly ubiquitinated by MDM2 to promote its degradation by the proteasome. **b** After nucleolar stress (drug-induced or caused by genetic mutations/ribosomopathies), ribosome synthesis is impaired, and a

larger amount of free 5S particles accumulate in the nucleoplasm. The extra free 5S particles can then be recognized by MDM2, which can no longer ubiquitinate p53, thereby stabilizing p53 and promoting cell cycle arrest. **c** In cells lacking SURF2, nucleolar stress still impairs ribosome synthesis, but this time, even more, free 5S RNPs are able to bind to MDM2, inducing stronger stabilization and activation of p53, followed by more cell cycle arrest. **d** In contrast, in cells overexpressing SURF2, nucleolar stress promotes free 5S RNP accumulation in the nucleoplasm, all of which are recognized by SURF2, which competes with MDM2 for binding. As a result, MDM2 is free and ubiquitinates p53, conferring to these cells a capacity to resist to nucleolar stress.

particles accumulates in the nucleoplasm and cannot be buffered by SURF2 (Fig. 9b). In that case, free 5S RNP particles can bind MDM2 to promote p53 activation and cell cycle arrest. In the absence of SURF2, in normal conditions, any small amount of free 5S can induce p53 activation and affect the cell cycle. Upon nucleolar stress, a greater fraction of free 5S RNP accumulates in nucleoplasm compared to normal cells, which promotes an even stronger response to NS (Fig. 9c). In contrast, when SURF2 is overexpressed, free 5S particles released upon nucleolar stress are sequestered by SURF2, thus inhibiting their interaction with MDM2, which prevents p53 activation (Fig. 9d). This free 5S RNP buffering capacity of SURF2 could be hijacked by cancer cells to resist p53 activation upon nucleolar stress, hence its overexpression found in many cancers compared to healthy tissues (Supplementary Table S4).

This regulation of free 5S RNPs by SURF2 represents an additional layer of complexity in nucleolar stress response. Recently, other

studies highlight the role of another ribosomal protein, RPL22, in the control of p53 through regulating MDM2/MDMX/P53 pathway^{58,59}. How p53 is regulated by ribosomal proteins and their regulating partners upon nucleolar stress and how cells integrate these different signals remain understudied. The capacity of SURF2 to regulate NS response, on the other hand, opens up the possibility of highly innovative therapeutic strategies in order to increase cancer cell sensitivity to chemotherapeutic drugs since most of them rely on NS to activate p53 and cell cycle arrest and further induce cell death. It is of particular interest to notice that co-treatment of U2OS cells by Actinomycin D and SURF2 siRNAs induce cell death, whereas taken individually at low concentrations, these treatments only promote cell cycle arrest. In order to test how SURF2 expression could affect the phenotypic traits of cancer cells, we used wound healing assays and observed that SURF2 knock-out impedes cancer cells capacity to migrate, whereas its overexpression increases cells capacity to migrate upon NS (Fig. 7a, b).

Furthermore, typical drawbacks of anticancer chemotherapies are their associated secondary effects. Hence, finding a way to reduce drug dosage by specifically increasing cancerous cell sensitivity to stress (without affecting pathways equally important for healthy cells, such as ribosome production), could represent a means of increasing the therapeutic window and reducing adverse effects. It could also represent a first line of treatment for some cancer types. In our Pan-Cancer study, we found that high levels of SURF2 are associated with poor overall survival in a specific cancer, adrenocortical carcinoma, a rare endocrine tumor (Fig. 3a, b, d, e, and Supplementary Table S5). Although this specific relation is yet to be understood, it is interesting to notice that among the top pathways deregulated upon SURF2 depletion, we found hormonal pathways that play a major role in this cancer etiology (Table S8)⁶⁰. In this cancer, SURF2 expression can be used as an independent prognostic marker, positioning SURF2 both as a good prognostic marker and anti-cancer therapeutic target and a prognostic marker. Interestingly, a recent study predicts that 26% of adrenocortical cancer patients could benefit from MDM2 inhibitors to reactivate the p53 pathway, a major driver of adrenocortical tumor⁶¹. Of note, another study underlines the link between 5S RNPs homeostasis and HCC cancers, suggesting a particular link between some cancers and 5S RNPs metabolism, which needs to be studied in depth²⁵.

Free 5S RNPs homeostasis is also key in a group of diseases originating from ribosome production defects and regrouped as ribosomopathies³³. In Diamond-Blackfan Anemia (DBA), a well-characterized ribosomopathy, activation of p53 by free 5S particles is likely at the core of the etiology of these diseases since some symptoms are linked to early p53 activation, such as growth retardation, developmental problems and even erythropoiesis failure^{62–64}. In addition, the patients suffering from these diseases show a higher cancer incidence compared to the general population. Hence, DBA is associated with a 30-fold increased risk of developing acute myeloid leukemia (AML), osteosarcoma, or colon cancer⁶⁵. Recently, two different studies on patients suffering from Shwachman-Diamond syndrome (SBDS), another ribosomopathy due to mutations in the pre-60S subunit assembly factor SBDS, nicely demonstrated how patients first harbor hypo-proliferative patterns due to SBDS mutations, then acquire compensatory mutations in TP53 to escape the growth selective pressure, and thus develop a pre-malignant cancer state^{66–68}. There again, studying how SURF2 could participate in the etiology of these rare diseases and how its expression is regulated during development represent interesting research prospects.

Of note, over-expression of SURF2 in U2OS cells does not seem to alter ribosome synthesis or cell fitness as seen by cell cycle analysis (Supplementary Fig. S3). First, this observation allows for therapeutic strategies development. Second, this implies that 5S RNP integration into ribosomes is not affected by SURF2 over-expression, suggesting that SURF2 only interacts with free 5S RNPs that are released from or not integrated into pre-ribosomes. How free 5S RNP particles interact with their different partners and how this is regulated in cells remains to be elucidated.

In summary, the work presented here demonstrates how free 5S RNP is key in cell stress response, and highlights SURF2 as a regulator of this response. With this capacity, it could represent a therapeutic target to increase cancer cells sensitivity to chemotherapeutic drugs and as a prognostic marker in adrenocortical carcinomas. Moreover, its overexpression could impede free 5S RNP function to reduce p53-associated symptoms in genetic diseases, which represents an interesting therapeutic strategy for diseases such as ribosomopathies, a hypothesis that needs to be explored further. However, how SURF2 exerts its molecular function on free 5S RNP and how it is regulated in cells remains to be elucidated. Moreover, although our study provides solid data on SURF2 function in U2OS cells and on some aspects in other cell lines, functional characterization of this factor in other cell types and integrated models is required.

Methods

Cell lines

The U-2OS Flp-In T-Rex cell lines were produced according to the manufacturer's instruction (Invitrogen/Thermo Fisher). The cDNAs of RPL5 or SURF2 were cloned into a pcDNA5-FRT-TO vector to enable expression of the protein with a C-terminal 2xFLAG-PreScission protease site-His6 (FLAG) tag. Alternatively, the cDNA of SURF2 was fused to the EGFP tag and cloned into pcDNA5-FRT-TO plasmid. These plasmids or the empty plasmids (control) were co-transfected with a pOG44 plasmid into Flp-In T-Rex U-2OS cells, and cells that had stably integrated the plasmid into their genome were selected and maintained using hygromycin B and maintained using hygromycin B (30 µg/ml) and blasticidin (30 µg/ml). The expression of proteins was induced with tetracyclin (1 µg/mL; Sigma-Aldrich, T7660).

All the cell lines were maintained in high-glucose Dulbecco's modified Eagle's medium supplemented with 10% fetal bovine serum and 1 mM sodium pyruvate. The cells were incubated at 37 °C in a humidified incubator containing 5% CO₂. Cells were treated with following drugs with the indicated concentrations: Actinomycin D (10 nM or 400 nM 24 h); 5-Fluorouracil (50 µM or 500 µM 24 h); Doxorubicin (100 nM 24 h); BMH-21 (150 nM 36 h or 5 µM 24H); Staurosporine (25 nM 24 h); MG132 (10 µM 24H).

A pool of four siRNA duplexes from Eurogentec was used to target SURF2 mRNA (CUG-CAA-GUG-AUG-ACA-GCA-U/AUG-CUG-UCA-UCA-CUU-GCA-G, GGA-GGG-AGG-ACC-AGA-UGG-A/UCC-AUC-UGG-UCC-UCC-CUC-C, AAG-CAC-AUG-CCG-UGA-AGU-U/AAC-UUC-ACG-GCA-UGU-GCU-U and CCA-GCG-AGC-UCU-GUG-UAA-A/UUU-ACA-CAG-AGC-UCG-CUG-G. On duplex for RPL11 mRNA AAG-GUG-CGG-GAG-UAU-GAG-UUA/UAA-CUC-AUA-CUC-CCG-CAC-CUU and on duplex for RPL5 mRNA GCC-ACA-AUG-UUG-CAG-AUU-A/UAA-UCU-GCA-ACA-UUG-UGG-C were used. Each siRNA solution was added at a final concentration of 5 µM to 10 × 10⁶ cells diluted in ZAP buffer (10 mM sodium phosphate buffer, pH 7.25, containing 250 mM sucrose and 1 mM MgCl₂). Electroporation was performed at 240 V with a Gene Pulser (Bio-Rad). After 5 min incubation at RT, cells were plated and grown at 37 °C for 48 h. Depletion of SURF2 was completed with a second round of siRNA treatment (96 h total). Control cells were electroporated with a scramble siRNA (siRNA-negative control duplex; Eurogentec).

Label-free quantitative proteomics

Protein preparation for 5S particle partner identification. For the proteome analysis, cells were prepared in quadruple biological replicates for four conditions: (i) U2OS cells (control); (ii) U2OS cells overexpressing RPL5-flag; (iii) control cells treated with Actinomycin D; (iv) U2OS cells overexpressing RPL5-flag and treated with actinomycin D (10 ng/mL, Sigma-Aldrich A9415). RPL5-Flag proteins and associated complexes were immunoprecipitated using the same protocol as "proteins immunoprecipitation after sucrose cushion" until the elution step. Trapped proteins on anti-Flag beads were eluted using Flag buffer (20 mM Tris-HCl pH 7.5, 200 mM NaCl, 5 mM MgCl₂) supplemented with 0.4 mg/mL 2xflag peptide (H-MDYKDDDDKGT-DYKDDDDKG-OH, Schafer), precipitated by TCA (Sigma-Aldrich, T9159) and glycogen (Thermo Scientific, R0551) and re-suspended in a buffer containing 20 mM Tris-HCl pH 7.5, 200 mM NaCl, 5 mM MgCl₂, 5% glycerol, 5% SDS. Then the protocol "Trypsin digestion and mass spectrometry analysis" was followed.

Protein preparation for SURF2 partners identification. For the proteomic analysis, U2OS control cells were prepared in quadruple biological replicates for two conditions: (i) GAPDH immunoprecipitation and (ii) SURF2 immunoprecipitation. Cells were harvested, washed with PBS with 1 mM EDTA, resuspended in buffer E (20 mM Tris-HCl pH 7.5, 200 mM NaCl, 5 mM MgCl₂, 0.5 mM EDTA, 0.2% Triton, 1 mM DTT, complete protease inhibitor cocktail (Roche), RNase ribonuclease

inhibitor (Promega, N261B)) and disrupted with a Bioruptor Sonicator by sonication (2 min, 5 s/5 s on/off, 20% amplitude). Cell debris was removed by centrifugation (10 min, 14,000 × *g*, 4 °C). Protein concentrations of the extracts were determined using a Bio-Rad protein assay kit (Biorad, 5000006). The same amounts of proteins were incubated with antibodies (anti-SURF2 or anti-GAPDH antibodies) coupled to protein G sepharose beads (Cytiva, 17061801) for 2 h at 4 °C. After immunoprecipitation, beads were washed three times with buffer E (20 mM Tris-HCl pH 7.5, 200 mM NaCl, 5 mM MgCl₂, 0.5 mM EDTA, 0.2% Triton, 1 mM DTT) and the associated proteins were eluted with 2X buffer (100 mM Tris-HCl pH 7.5, 10% glycerol, 10% SDS). Then the protocol “*Trypsin digestion and mass spectrometry analysis*” was followed.

Trypsin digestion and mass spectrometry analysis. Disulfide bonds were reduced with 25 mM DTT for 5 min at 95 °C under agitation, followed by alkylation of cysteine residues in 60 mM iodoacetamide for 30 min in the dark at room temperature. Each reduced/alkylated protein sample was then digested using the S-Trap™ Mini spin column protocol⁶⁹. Briefly, the undissolved matter was removed by centrifugation for 8 min at 13,000 × *g*. 12% aqueous phosphoric acid was added at 1:10 to the protein sample for a final concentration of ~1.2% phosphoric acid, followed by seven volumes of S-Trap binding buffer (90% methanol, 100 mM TEAB, pH 7.1). After gentle mixing, the protein solution was loaded onto an S-Trap filter by centrifugation at 4000 × *g*. Afterward, the captured proteins were washed six times with 400 μL S-Trap binding buffer. Digestion was performed overnight at 37 °C by the addition of 20 μL of trypsin (Sequencing Grade Modified Trypsin, Promega) at 37.5 ng/μL in 50 mM ammonium bicarbonate. The digested peptides were eluted by the addition of 40 μL of 50 mM ammonium bicarbonate, followed by 40 μL of 0.2% formic acid (FA), and finally 35 μL of 50% aqueous acetonitrile containing (ACN) 0.2% FA. Each elution was performed at 4000 × *g* for 1 min. The different eluates were pooled together, dried down, resuspended in 20 μL of 0.05% trifluoroacetic acid (TFA) in 2% ACN, and sonicated for 10 min before analyzing by online nanoLC using an UltiMate® 3000 RSLCnano LC system (ThermoScientific, Dionex) coupled to an Orbitrap Fusion™ Tribrid™ mass spectrometer (Thermo Scientific, Bremen, Germany) operating in positive mode. 200 ng of each sample were loaded onto a 300 μm ID × 5 mm PepMap C18 pre-column (Thermo Scientific, Dionex) at 20 μL/min in 2% ACN, 0.05% TFA. After 3 min of desalting, peptides were online separated on a 75 μm ID × 50 cm C18 column (in-house packed with Reprosil C18-AQ Pur 3 μm resin, Dr. Maisch; Proxeon Biosystems, Odense, Denmark) equilibrated in 90% of buffer A (0.2% FA), with a gradient of 10 to 30% of buffer B (80% ACN, 0.2% FA) for 100 min then 30% to 45% for 20 min at a flow rate of 300 nL/min. The instrument was operated in data-dependent acquisition (DDA) mode using a top-speed approach (cycle time of 3 s). Survey scans MS were acquired in the Orbitrap over 350–1400 *m/z* with a resolution of 120,000 (at 200 *m/z*), an automatic gain control (AGC) target value of 4e5, and a maximum injection time of 60 ms. Most intense multiply charged ions (2+ to 6+) per survey scan were selected at 1.7 *m/z* with quadrupole and fragmented by Higher Energy Collisional Dissociation (HCD). The monoisotopic precursor selection was turned on, the intensity threshold for fragmentation was set to 25,000, and the normalized collision energy was set to 28%. The resulting fragments were analyzed in the Orbitrap with a resolution of 30,000 (at 200 *m/z*), an automatic gain control (AGC) target value of 5e4 and a maximum injection time of 54 ms. Dynamic exclusion was used within 60 s with a 10 ppm tolerance, to prevent repetitive selection of the same peptide. For internal calibration, the 445.120025 ion was used as lock mass.

MS-based protein identification. Acquired MS and MS/MS data as raw MS files were converted to the mzDB format using the pwiz-mzdb converter (version 0.9.10, <https://github.com/mzdb/pwiz-mzdb>)

executed with its default parameters⁷⁰. Generated mzDB files were processed with the mzdb-access library (version 0.7, <https://github.com/mzdb/mzdb-access>) to generate peaklists. Peak lists were searched against the UniProtKB/Swiss-Prot protein database with homo sapiens taxonomy in the Mascot search engine (version 2.6.2, Matrix Science, London, UK). Cysteine carbamidomethylation was set as a fixed modification and methionine oxidation as a variable modification. Up to two missed trypsin/P cleavages were allowed. Mass tolerances in MS and MS/MS were set to 10 ppm and 0.6 Da, respectively. Validation of identifications was performed through a false-discovery rate set to 1% at protein and peptide-sequence match level, determined by target-decoy search using the in-house-developed software Proline software version 1.6⁷¹. The mass spectrometry proteomics data have been deposited to the ProteomeXchange Consortium via the PRIDE¹ partner repository with the dataset identifier PXD047905.

RNA-seq analysis

Total RNA extraction. U2OS cells were treated with either siSCR or siSURF2 siRNAs for 96 h in 10 cm dishes, with three independent replicates. Total RNAs were extracted with TRizol following the manufacturer's procedure. The total RNA concentration and RNA integrity of each sample were determined with NanoDrop and Qubit 4 Fluorometer (Thermo Fisher Scientific). RNASeq library preparations and sequencing reactions were conducted by GENEWIZ.

Bioinformatics. Initial bioinformatics analysis of the RNASeq was conducted by GENEWIZ. Briefly, data was generated with an Illumina HiSeq 2 × 150 PE HO configuration. Sequence reads were trimmed to remove adapter sequences and nucleotides with poor quality (Trimomatic v.0.36). Using the STAR aligner v.2.5.2b, the trimmed reads were mapped to the Homo sapiens GRCh38p13 reference genome available on ENSEMBL. Gene expression between distinct groups was compared using the DESeq2 package. The Wald test was used to generate *P*-values and log₂ fold changes. Genes with an adjusted *P*-value < 0.05 and absolute log₂ fold change > 1 were called differentially expressed genes for each comparison. Raw data are deposited on the GEO service (GSE267134).

For the GSEA analysis, the GSEA software package (Desktop v4.3.3) developed by the MIT/BROAD Institute was used. Gene sets H.all.v2023.2.Hs.symbols.gmt was used. All gene set files for this analysis were obtained from the GSEA website www.broadinstitute.org/gsea/. An enrichment map was used for the visualization of the GSEA results. GSEA computes four key statistics for the gene set enrichment analysis. GSEA *P*-values were derived from permutation testing and corrected for multiple testing using the False Discovery Rate (FDR) method. Enrichment score (ES) and FDR value were applied to sort SURF2 depleted and control cells genes-enriched after gene set permutations were performed 1000 times for the analysis. Gene Network Analysis was based on DEGs (log₂foldchange > 1).

Immunoblotting assays

Protein extraction was done in ice-cold lysis buffer (1% Triton, 50 mM Tris-HCl pH 7.4, 200 mM NaCl, 1 mM EDTA, and a complete protease inhibitor cocktail (Roche)). Protein concentrations of the extracts were determined using a Bio-Rad protein assay kit (Biorad, 5000006). Proteins were diluted in Invitrogen 2X sample buffer (NuPAGE™ LDS Sample Buffer (4X) (NP0007) and NuPAGE™ Sample Reducing Agent (10X) (NP0009)) and 20 μg/lane of protein were loaded on NuPAGE™ 4 to 12%, Bis-Tris protein gels (Invitrogen, NP0321BOX) and transferred to nitrocellulose membrane using the Trans-Blot Turbo Transfer System from Biorad. Membranes were immunoblotted with a primary antibody, followed by incubation with a secondary antibody coupled with HRP (Promega anti-rabbit (W401B) or anti-mouse HRP (W401B)) (dil: 1/10,000). The blots were visualized using the Clarity Western ECL kit from Biorad. The following antibodies were used: p53 (dil: 1/1000)

(Invitrogen, MA5-12557 (DO7)), p21(dil: 1/1000) (CDKN1A/p21CIP1 AB clonal, A2691), SURF2 (dil: 1/1000) ((Bethyl lab, A304-611A), Flag (dil: 1/1000) (MERCK, F3165), GAPDH (dil: 1/1000) (Genetex, GTX627408), RPL11 (dil: 1/1000) (Invitrogen, 37-3000), RPL5 (dil: 1/1000) (Invitrogen, PA5-102539), RPL17 (dil: 1/1000) (Gentech, GTX111934), Fibrillarlin (collaborators), MDM2 (dil: 1/1000) (SMP14 Santa Cruz, SC965), Actin (dil: 1/1000) (Sigma, A4700).

Cell cycle assays

The cell cycle was analyzed by flow cytometry. Cells were harvested by trypsinization, fixed in 70% ethanol, and stained with DAPI (1 µg/ml; Sigma, D9542) in PBS completed with RNase A (100 µg/ml, Thermo Scientific, EN0531) for 30 min at RT. Samples were then analyzed for their DNA content using CytoFLEX S Flow Cytometer and CytExpert software.

Apoptosis assays

Cell death was quantified by using the Annexin V-FITC & Propidium Iodide (PI) Dead Cell Apoptosis kit from Invitrogen (V13242). In brief, cells depleted for SURF2 and treated with the indicated drugs were harvested and washed in cold PBS. Then, 1×10^5 cells were resuspended in 100 µl of incubation buffer containing Annexin V-FITC and propidium iodide (PI) and incubated in the dark for 15 min. Data were acquired on a CytoFLEX S Flow Cytometer and CytExpert software.

Viability assays

Cells depleted for SURF2 were plated in 6 well culture dishes. After 12 h, cells were treated with actinomycin D (10 ng/mL, Sigma-Aldrich A9415) then, at each time point, cells were incubated with 400 µL of 1% crystal violet staining solution (Sigma-Aldrich, V5265) for 20 min at RT. Cells were washed 2 times with PBS, and 3 pictures were taken under the microscope. Then, crystal violet was resolubilized with 33% acid acetic and diluted into 96 well plates to read optical density OD595 with a plate reader.

Northern-blot assays

Total RNAs were extracted with Trizol from cell pellets containing 20×10^6 cells. The aqueous phase was extracted with phenol-chloroform-isoamyl alcohol (25:24:1; Sigma), then with chloroform. Total RNAs were recovered after precipitation with 2-propanol. For northern blot analyses, 3 µg/lane of total RNAs were separated into two types of gels. Long RNAs were separated on a 1.2% agarose gel containing 1.2% formaldehyde and Tri/Tri buffer (30 mM triethanolamine, 30 mM tricine, pH 7.9). Small RNAs were separated on 6% polyacrylamide gel containing 7% urea and TBE buffer (90 mM Trizma base, 90 mM Boric acid, 2 mM EDTA). Then, RNAs were transferred to a Hybond N+ nylon membrane by a passive transfer overnight. Pre-hybridization was performed for 1 h at 45 °C in a buffer containing $6 \times$ SSC, $5 \times$ Denhardt's solution, 0.5% SDS, and 0.9 g/mL tRNAs). The 5'-radiolabeled oligonucleotide probe was incubated overnight. The sequences of the probes were: ITS1: CCT-CGC-CCT-CCG-GGC-TCC-GTT-AAT-GAT-C, ITS2: GCG-CGA-CGG-CGG-ACG-ACA-CCG-CGG-CGT, + CTG-CGA-GGG-AAC-CCC-CAG-CCG-CGC-A, 18S: CCG-GCC-GTC-CCT-CTT-AAT-CAT-GGC, 28S: CCC-GTT-CCC-TTG-GCT-GTG-GTT-TCG-CTG-GAT-A, 5.8S: GGG-GCG-ATT-GAT-CGG-CAA-GCG-ACG-CTC, 5S: CCU-CGC-CCU-CCG-GGC-UCC-GUU-AAU-GAU-C. Membranes were washed twice for 10 min in $2 \times$ SSC, 0.1% SDS, and once in $1 \times$ SSC, 0.1% SDS, and then exposed. Signals were acquired with a Typhoon Trio PhosphorImager (GE Healthcare) and quantified using the MultiGauge software.

Immunofluorescence assays

The expression of SURF2-GFP was induced to the same level of the endogenous SURF2 protein (tetracycline at 5 ng/mL for 24 h). Cells were seeded in 12-well plates on microscope cover glasses and grown

for 24 h. Cells were fixed with 4% paraformaldehyde for 5 min, permeabilized with (0.1% Triton X-100 and 0.02% SDS in PBS). Fixed cells were incubated in blocking solution 2% BSA in PBS for 30 min and incubated overnight at 4 °C with anti-fibrillarlin antibodies at 1:200. Cells were washed 3 times for 5 min with (2% BSA in PBS), and subsequently incubated for 30 min with secondary antibodies (Alexa Fluor goat anti-mouse IgG (H+L)/Alexa Fluor 647 secondary antibody (Invitrogen, A21236) at 1:1000. After 3 washes, cells were incubated briefly in 0.1% Triton X-100, 0.02% SDS in PBS, and post-fixed with 4% PFA in PBS. Cells were incorporated with DAPI (1 µg/mL, Sigma, D9542) for 10 min. After washes with PBS, coverslips were mounted in Mowiol. Imaging was performed on a Leica TCS SP8 MP Multiphoton microscope. Images were captured in confocal mode using the x63 objective. Image analyses were performed using ImageJ software.

Sucrose sedimentation profiling

Buffers contain cycloheximide (10 µg/mL, Merck, C7698) at each step of this protocol. 50×10^6 cells were harvested and resuspended in a lysis buffer (10 mM Hepes KOH, pH 7.9, 1.5 mM MgCl₂, 10 mM KCl, 1 mM DTT, 10 µg/mL cycloheximide). Then cells were homogenized with a Dounce tissue grinder on ice with a tight pestle and centrifuged at $1000 \times g$ for 10 min at 4 °C. The top soluble phase was clarified through two centrifugations at $10,000 \times g$ for 15 min at 4 °C. Supernatants were collected, and protein concentrations were determined using a Bio-Rad protein assay kit (Biorad 5000006). 750 µg of extracts were loaded on a 10–50% sucrose gradient. Gradients were centrifuged at $250,00 \times g$ for 2 h at 4 °C in an Optima L-100XP ultracentrifuge (Beckman-Coulter). Following centrifugation, the fractions were collected using a Foxy Jr fraction collector (Teledyne ISCO), and the absorbance at 254 nm was measured with a UA-6 device (Teledyne ISCO). For protein analyses, 250 µL of each fraction were precipitated with TCA (Sigma-Aldrich, T9159) and glycogen (Thermo Scientific, R0551), and protein pellets were resuspended in Invitrogen 2X sample buffer (NuPAGE™ LDS Sample Buffer (4X) (NP0007) and NuPAGE™ Sample Reducing Agent (10X) (NP0009)).

Cell fractionation following the PSE method

Cells were harvested by scrapping with PBS and pelleted by centrifugation. Cells were gently resuspended in SN1 buffer (20 mM HEPES-NaOH (pH 7.5), 130 mM KCl, 10 mM MgCl₂, 0.05% Igepal, 600 U/mL RNasin ribonuclease inhibitor (Promega, N261B)) completed with cOmplete protease inhibitor (1/30) (Roche) and centrifuged ($1300 \times g$, 3 min, 4 °C). SN1 supernatants were collected and proteins were diluted in Invitrogen 2X sample buffer (NuPAGE™ LDS Sample Buffer (4X) (NP0007) and NuPAGE™ Sample Reducing Agent (10X) (NP0009)). SN1 was then stored at –80 °C. The previous pellets of cellular extracts were vortexed with SN1 buffer and spined down ($1300 \times g$, 3 min, 4 °C). The supernatants were eliminated, and the pellets were resuspended in SN2 buffer (10 mM HEPES-NaOH (pH 7.5), 10 mM NaCl, 5 mM MgCl₂, 0.1% Igepal, 0.5 mg/mL heparin, 600 µ/ml RNasin ribonuclease inhibitor (Promega, N261B)) completed with DNase I (Invitrogen, 18068015), then incubated 10 min at RT with gentle mixing. Extracts were centrifuged ($12,500 \times g$, 10 min, 4 °C). SN2 supernatants were collected, and proteins were diluted in Invitrogen 2X sample buffer (NuPAGE™ LDS Sample Buffer (4X) (NP0007) and NuPAGE™ Sample Reducing Agent (10X) (NP0009)). SN2 was then stored at –80 °C. Finally, remaining pellets of cellular extracts were resuspended with SN3 buffer (20 mM HEPES-NaOH (pH 7.5), 200 mM NaCl, 4 mM EDTA, 0.1% Igepal, 0.04% sodium deoxycholate, 4 mM imidazole, 0.1 mg/ml heparin, 1 mM DTT, cOmplete protease inhibitor (1/100), 600 µ/ml RNasin ribonuclease inhibitor (Promega, N261B)) and mixed for 20 min at RT. Extracts were centrifuged ($12,500 \times g$, 10 min, 4 °C). SN3 supernatants were collected, and proteins were diluted in Invitrogen 2X sample buffer (NuPAGE™ LDS Sample Buffer (4X) (NP0007) and NuPAGE™ Sample Reducing Agent (10X) (NP0009)).

(NP0009)). SN3 was then stored at -80°C . Proteins were analyzed by western blots.

Proteins and RNA immunoprecipitation after sucrose cushion

Cells were harvested, washed with 1 mM EDTA in PBS, resuspended in buffer E (20 mM Tris-HCl pH 7.5, 200 mM NaCl, 5 mM MgCl₂, 0.5 mM EDTA, 0.2% Triton, 1 mM DTT, complete protease inhibitor cocktail (Roche), RNasin ribonuclease inhibitor (Promega, N261B)) and disrupted with a Bioruptor Sonicator by sonication (2 min, 5 s/5 s on/off, 20% amplitude). Cell debris was removed by centrifugation (10 min, $14,000 \times g$, 4°C). Protein concentrations of the extracts were determined using a Bio-Rad protein assay kit (Biorad, 5000006). The same amounts of proteins were loaded on a double sucrose cushion (20% and 30% sucrose) and centrifuged at $190,000 \times g$ for 2 h at 4°C in an Optima L-100XP ultracentrifuge (Beckman-Coulter). Extracts were incubated with pre-washed anti-Flag beads (Sigma, A2220) or with antibodies (anti-SURF2 or anti-MDM2 antibodies) coupled to protein G sepharose beads (Cytiva, 17061801) for 2 h at 4°C . 10% of inputs were conserved, precipitated with TCA (Sigma-Aldrich, T9159) and glycogen (Thermo Scientific, R0551), pellets were resuspended with Invitrogen 2X sample buffer (NuPAGE™ LDS Sample Buffer (4X) (NP0007) and NuPAGE™ Sample Reducing Agent (10X) (NP0009)) or total RNAs were extracted following phenol-chloroform and GTC method. After immunoprecipitation, beads were washed three times with Flag buffer (20 mM Tris-HCl pH 7.5, 200 mM NaCl, 5 mM MgCl₂), and the associated proteins were eluted with Invitrogen 2X sample buffer (NuPAGE™ LDS Sample Buffer (4X) (NP0007) and NuPAGE™ Sample Reducing Agent (10X) (NP0009)). For RNA, after being washed, RNA was extracted following phenol-chloroform and GTC method. RNAs were then analyzed on a 15% acrylamide-8M Urea followed by Northern-blot analyses.

^[5-32P]pCp labeling of immunoprecipitated RNAs

Cells were harvested in TBS buffer (150 mM NaCl, 40 mM Tris-HCl pH 7.4), resuspended in lysis buffer (150 mM NaCl, 0.05% Igepal, 50 mM Tris-HCl pH 7.4, 5 mM MgCl₂) completed with complete protease inhibitor cocktail (Roche) and disrupted with a Bioruptor Sonicator by sonication (2 min, 5 s/5 s on/off, 20% amplitude). Cell debris was removed by centrifugation at $16,000 \times g$ for 10 min, and the clarified extracts were incubated with antibodies (anti-SURF2 or anti-HEXIM1 antibodies) coupled to protein G sepharose beads (Cytiva, 17061801) for 2 h at 4°C . Then, beads were washed 3 times, and immunoprecipitated RNAs were extracted using the phenol-chloroform protocol. RNAs were incubated with ^[5-32P]pCp and T4 RNA ligase (Promega, M1051) O/N at 4°C . Then RNAs were precipitated with ammonium acetate and ethanol for 10 min at -70°C and pelleted by centrifugation (10 min, $13,000 \times g$). RNA pellets were washed with 70% ethanol and recovered with a formamide loading buffer. Then, a loading dye buffer was added, and RNA was analyzed on a 12% acrylamide gel.

In vitro pull-down assays

The cDNAs of the SURF2 or SURF2(I-136) were cloned into pScodon plasmid (open biosystem) in translational fusion with HIS⁶ (His tag). RPL5 or RPL11 cDNAs were synthesized by Genscript and cloned into pGEX-6T. The expression and purification were essential, as described⁷². Briefly, the proteins were expressed in the BL21 strain from *Escherichia coli* at 37°C in LB medium (Sigma) supplemented with 100 μg/mL ampicillin until OD₆₀₀ between 0.4 and 0.5. Recombinant protein expression was induced by adding 1 mM isopropyl-β-D-1-thiogalactopyranoside, incubating overnight at 20°C , harvesting by centrifugation, and cell pellets were frozen at -20°C . Cells pellets were resuspended in buffer A (300 mM NaCl, 20 mM Tris-HCl pH 8.0, 0.5 mM EDTA, 10 mM B-mercaptoethanol, 10% glycerol, tablet Roche, 5 mM Imidazole) supplemented with complete EDTA-free protease inhibitors (Roche). Cells were lysed by sonication, and lysate was

centrifuged at $38,000 \times g$ for 30 min. The cleared lysates were mixed as indicated for 2 h at 4°C . The mix was then loaded on glutathione-sepharose beads pre-equilibrated with buffer A (300 mM NaCl, 20 mM Tris-HCl pH 8.0, 0.5 mM EDTA, 10 mM B-mercaptoethanol, 10% glycerol, tablet Roche, 5 mM Imidazole) and mixed for 2 h at 4°C . Beads were then washed 4 times with buffer A and resuspended in loading dye (1X LDS with denaturing reagent from Invitrogen) and loaded on Nu-PAGE 4–12% gels using 1X MOPS as running buffer.

Wound-healing assays

4.5 to 5×10^5 cells were seeded in 6-well plates. After 48 h of growth, the confluent cell monolayer was ablated with a 20 μL tip. The wells were then rinsed 3x with PBS 1X and incubated in DMEM supplemented with 3% SVF at 37°C . When indicated, cells were then treated with 0.5 μg/mL tetracycline per well. Images were taken at the EVOS Fluid cell imaging station at T0h and T24h. Scar size was analyzed by ImageJ software using the Wound_Healing_size_tool.

Database

Different databases were used to perform analyses, either directly using the portal or exporting the data of interest.

GTEx: (<https://gtexportal.org/home/>) Genotype-Tissue Expression is a public platform containing molecular data of healthy tissues derived from people of all ages, genders, and ethnicity.

TCGA: (<https://www.cancer.gov/ccg/research/genome-sequencing/tcga>) The Cancer Genome Atlas is a public database compiled from the National Cancer Institute's CDM portal. It includes 33 cancers from 11,000 patient samples over 12 years and contains annotated clinical data and molecular data.

TARGET: (<https://www.cancer.gov/ccg/research/genome-sequencing/target/about>) therapeutically Applicable Research to Generate Effective Treatments is a public platform dedicated to molecular characterization of pediatric cancers with available clinical, genomic, and transcriptomic data.

cBioPortal: (<https://www.cbioportal.org/>) This public portal contains data from over 300 multidimensional studies in open-access. It includes genomic, transcriptomic, molecular, and clinical data from multiple datasets. It allows exploratory analysis and corresponds to a global visualization web tool, which includes the exportation of data from TCGA, TARGET, ICGC, and other individual datasets. The raw data are not directly downloadable on the portal.

XENA UCSC: (<https://xena.ucsc.edu/>) The University of California Santa Cruz (UCSC) Xena browser. This public data portal contains over 1500 datasets and 50 different types of cancers with clinical, genomic, transcriptomic, and other types of data. It enables interactive exploratory analysis and exportation of accurate data of interest from TCGA, ICGC, GDC, TARGET, GTEx, and other databases.

DEPMAP: (<https://depmap.org/portal/>).

Statistical Analysis

Label-free quantitative proteomics analysis. Proteins enriched over 2-fold with a p -value below 0.05 were considered significantly enriched. For label-free relative quantification across samples, raw MS signal extraction of identified peptides was performed using Proline⁷¹. The cross-assignment of MS/MS information between runs was enabled, allowing the assigned peptide sequences to detect non-identified features. Each protein intensity was based on the sum of unique peptide intensities and was normalized across all samples by the median intensity. Missing values were independently replaced for each run by its 5% quantile. For each pairwise comparison, an unpaired two-tailed Student's t test was performed, and proteins were considered significantly enriched when their absolute log₂-transformed fold change was higher than 1 and their p -value lower than 0.05. To eliminate false-positive hits from quantitation of low-intensity signals, two additional criteria were applied: only the proteins identified with a

total number of averaged peptide spectrum match (PSM) count > 4 and quantified in a minimum of two biological replicates, before missing value replacement, for at least one of the two compared conditions were selected. The *p*-value and fold change were calculated between the IP groups from RPL5_Flag overexpressing cells and the control IP groups (IPs with the α -flag antibody). The same statistical analysis was performed on equivalent IP groups resulting from cells incubated with Actinomycin D for 24 h. Volcano plots were drawn to visualize significant protein abundance variations between conditions in the presence or absence of drug. They represent $-\log_{10}$ (*p*-value) according to the \log_2 ratio. The complete list of proteins identified and quantified in immunopurified samples and analyzed according to this statistical procedure is described in the Supplementary file (Supplementary Tables S1, S2, and S3).

General data analysis. Data are expressed as means \pm SD. All statistical data ($n \geq 3$) were calculated using GraphPad Prism. Statistical details and significance reports can be found in the corresponding figure legends. No data were excluded from the analyses. The experiments were not randomized. The Investigators were not blinded to allocation during experiments and outcome assessment.

PanCancer analysis. Datasets were uploaded from the XENA UCSC portal (<https://xena.ucsc.edu/>) that compiled normalized gene expression levels from normal (GTEx) and tumoral (TCGA) tissues, as well as related clinical and genomic data of tumoral tissues (Goldman et al., Nat Biotechnol 2020; GTEx consortium, Nat Genet 2013; Grossman et al., New England J Medicine 2016). After data export and transformation, tumor datasets were built by conserving only tumoral tissues collected at diagnosis from non-metastatic patients. Quality control was performed to verify the normal distribution of the gene expression dataset (Shapiro test) or cohort consistency (follow-up median, survival association with gold standards such as metastatic relapse). The comparison of gene expression between two conditions was assessed using a non-parametric test (Wilcoxon test). Survival was investigated by plotting Kaplan-Meier survival curves and log-rank tests using the median as a cut-off of gene expression. Overall survival (OS) corresponds to the length of time from the date of cancer diagnosis to the date of death or censoring, while Progression-Free survival (PFS) corresponds to the length of time from the date of cancer diagnosis to the date of progression (i.e., death or local/distant relapse) or censoring. A Cox regression model was performed to compare the impact of SURF2 expression on key clinical parameters using a multivariate analysis. Lower SURF2 expression, absence of TP53 mutation, and tumor stage I were used as a reference for the analysis. *p*-values of the Wilcoxon tests and the log-rank tests were adjusted to multiple testing using the False Discovery Rate method. The statistical significance was based on a *p*-value < 0.05, where the H0 hypothesis is rejected. Statistics and visualization were performed using R studio (version 2024.04.1 + 748).

Reporting summary

Further information on research design is available in the Nature Portfolio Reporting Summary linked to this article.

Data availability

Uncropped blots and measurements used to generate graphs are provided as a Source Data file. Generated datasets can be found on publicly available repositories. The mass spectrometry proteomics data have been deposited to the ProteomeXchange Consortium via the PRIDE¹ partner repository with the dataset identifier [PXD047905](https://www.ebi.ac.uk/pride/archive/study/ PXD047905). RNA-seq raw data are deposited on the GEO service with accession number [GSE267134](https://www.ncbi.nlm.nih.gov/geo/query/acc.cgi?acc=GSE267134). Data and materials availability All data are available in the main text or the supplementary materials. Source data are provided in this paper.

References

- Zhong, L. et al. Small molecules in targeted cancer therapy: advances, challenges, and future perspectives. *Signal Transduct. Target Ther.* **6**, 201 (2021).
- Sabnis, A. J. & Bivona, T. G. Principles of resistance to targeted cancer therapy: Lessons from basic and translational cancer biology. *Trends Mol. Med.* **25**, 185–197 (2019).
- Montanaro, L., Treré, D. & Derenzini, M. Nucleolus, ribosomes, and cancer. *Am. J. Pathol.* **173**, 301–310 (2008).
- Derenzini, M. et al. Nucleolar size indicates the rapidity of cell proliferation in cancer tissues. *J. Pathol.* **191**, 181–186 (2000).
- Henras, A. K. et al. The post-transcriptional steps of eukaryotic ribosome biogenesis. *Cell. Mol. Life Sci.* **65**, 2334–2359 (2008).
- Albert, B. et al. A ribosome assembly stress response regulates transcription to maintain proteome homeostasis. *ELife* **8**, e45002 (2019).
- Mayer, C. & Grummt, I. Cellular stress and nucleolar function. *Cell Cycle* **4**, 1036–1038 (2005).
- Olson, M. O. J. Sensing Cellular Stress: Another New Function for the Nucleolus? *Sci. STKE* <https://doi.org/10.1126/stke.2242004pe10> (2004).
- Nicolas, E. et al. Involvement of human ribosomal proteins in nucleolar structure and p53-dependent nucleolar stress. *Nat. Commun.* **7**, 11390 (2016).
- Golomb, L. Volarevic, S. & Oren, M. p53 and ribosome biogenesis stress: the essentials. *FEBS Lett.* <https://doi.org/10.1016/j.febslet.2014.04.014> (2014).
- Donati, G., Peddigari, S., Mercer, C. A. & Thomas, G. 5S ribosomal RNA is an essential component of a nascent ribosomal precursor complex that regulates the Hdm2-p53 checkpoint. *Cell Rep.* **4**, 87–98 (2013).
- Domostegui, A. et al. Impaired ribosome biogenesis checkpoint activation induces p53-dependent MCL-1 degradation and MYC-driven lymphoma death. *Blood* **137**, 3351–3364 (2021).
- Pelletier, J. et al. Nucleotide depletion reveals the impaired ribosome biogenesis checkpoint as a barrier against DNA damage. *EMBO J.* **39**, e103838 (2020).
- Hannan, K. M. et al. Nuclear stabilization of p53 requires a functional nucleolar surveillance pathway. *Cell Rep.* **41**, 111571 (2022).
- Lindström, M. S., Bartek, J. & Maya-Mendoza, A. p53 at the crossroad of DNA replication and ribosome biogenesis stress pathways. *Cell Death Differ.* **29**, 972–982 (2022).
- Rubbi, C. P. Disruption of the nucleolus mediates stabilization of p53 in response to DNA damage and other stresses. *EMBO J.* **22**, 6068–6077 (2003).
- Zhou, X., Hao, Q., Liao, J., Zhang, Q. & Lu, H. Ribosomal protein S14 unties the MDM2-p53 loop upon ribosomal stress. *Oncogene* **32**, 388–396 (2013).
- Zhou, X., Liao, W.-J., Liao, J.-M., Liao, P. & Lu, H. Ribosomal proteins: functions beyond the ribosome. *J. Mol. Cell Biol.* **7**, 92–104 (2015).
- Yadavilli, S. et al. Ribosomal protein S3: A multi-functional protein that interacts with both p53 and MDM2 through its KH domain. *DNA Rep.* **8**, 1215–1224 (2009).
- Zhang, X. et al. Identification of ribosomal protein S25 (RPS25)-MDM2-p53 regulatory feedback loop. *Oncogene* **32**, 2782–2791 (2013).
- Marechal, V., Elenbaas, B., Piette, J., Nicolas, J. C. & Levine, A. J. The ribosomal L5 protein is associated with mdm-2 and mdm-2-p53 complexes. *Mol. Cell. Biol.* **14**, 7414–7420 (1994).
- Sloan, K. E., Bohnsack, M. T. & Watkins, N. J. The 5S RNP couples p53 homeostasis to ribosome biogenesis and nucleolar stress. *Cell Rep.* **5**, 237–247 (2013).
- Nishimura, K. et al. Perturbation of ribosome biogenesis drives cells into senescence through 5S RNP-mediated p53 activation. *Cell Rep.* **10**, 1310–1323 (2015).

24. Bursać, S. et al. Mutual protection of ribosomal proteins L5 and L11 from degradation is essential for p53 activation upon ribosomal biogenesis stress. *Proc. Natl. Acad. Sci. USA* **109**, 20467–20472 (2012).
25. Cao, P. et al. Genomic gain of RRS1 promotes hepatocellular carcinoma through reducing the RPL11-MDM2-p53 signaling. *Sci. Adv.* **7**, eabf4304 (2021).
26. Burger, K. et al. Chemotherapeutic drugs inhibit ribosome biogenesis at various levels. *J. Biol. Chem.* **285**, 12416–12425 (2010).
27. Derenzini, E., Rossi, A. & Treré, D. Treating hematological malignancies with drugs inhibiting ribosome biogenesis: when and why. *J. Hematol. Oncol.* **11**, 75 (2018).
28. Drygin, D. et al. Targeting RNA polymerase I with an oral small molecule CX-5461 inhibits ribosomal RNA synthesis and solid tumor growth. *Cancer Res.* **71**, 1418–1430 (2011).
29. Ferreira, R., Schneekloth, J. S., Panov, K. I., Hannan, K. M. & Hannan, R. D. Targeting the RNA polymerase I transcription for cancer therapy comes of age. *Cells* **9**, 266 (2020).
30. Khot, A. et al. First-in-human RNA polymerase I transcription inhibitor CX-5461 in patients with advanced hematologic cancers: Results of a phase I dose-escalation study. *Cancer Discov.* **9**, 1036–1049 (2019).
31. Baßler, J. & Hurt, E. Eukaryotic ribosome assembly. *Annu. Rev. Biochem.* **88**, 281–306 (2019).
32. Pestov, D. G., Strezoska, Z. & Lau, L. F. Evidence of p53-dependent cross-talk between ribosome biogenesis and the cell cycle: effects of nucleolar protein Bop1 on G(1)/S transition. *Mol. Cell. Biol.* **21**, 4246–4255 (2001).
33. Aubert, M., O'Donohue, M.-F., Lebaron, S. P.-E. Pre-ribosomal RNA processing in human cells: From mechanisms to congenital diseases. *Biomolecules* <https://doi.org/10.3390/biom8040123> (2018).
34. Lebaron, S. et al. Functionally impaired RPL8 variants associated with Diamond–Blackfan anemia and a Diamond–Blackfan anemia-like phenotype. *Hum. Mutat.* **43**, 389–402 (2022).
35. Oršolić, I. et al. Cancer-associated mutations in the ribosomal protein L5 gene dysregulate the HDM2/p53-mediated ribosome biogenesis checkpoint. *Oncogene* **39**, 3443–3457 (2020).
36. Zheng, J. et al. Structure of human MDM2 complexed with RPL11 reveals the molecular basis of p53 activation. *Genes Dev.* **29**, 1524–1534 (2015).
37. Miliani de Marval, P. L. & Zhang, Y. The RP-Mdm2-p53 pathway and tumorigenesis. *Oncotarget* **2**, 234–238 (2011).
38. Rinke, J. & Steitz, J. A. Precursor molecules of both human 5S ribosomal RNA and transfer RNAs are bound by a cellular protein reactive with anti-La lupus antibodies. *Cell* **29**, 149–159 (1982).
39. Steitz, J. A. et al. A 5S rRNA/L5 complex is a precursor to ribosome assembly in mammalian cells. *J. Cell Biol.* **106**, 545–556 (1988).
40. Kressler, D. et al. Synchronizing nuclear import of ribosomal proteins with ribosome assembly. *Science* **338**, 666–671 (2012).
41. O'Donohue, M.-F. et al. HEATR3 variants impair nuclear import of uL18 (RPL5) and drive Diamond-Blackfan anemia. *Blood* <https://doi.org/10.1182/blood.2021011846> (2022).
42. Castillo Duque de Estrada, N. M. et al. Structure of nascent 5S RNPs at the crossroad between ribosome assembly and MDM2-p53 pathways. *Nat. Struct. Mol. Biol.* **30**, 1119–1131 (2023).
43. Vassilev, L. T. et al. In vivo activation of the p53 pathway by small-molecule antagonists of MDM2. *Science* **303**, 844–848 (2004).
44. Duhig, T., Ruhrberg, C., Mor, O. & Fried, M. The human Surfeit locus. *Genomics* **52**, 72–78 (1998).
45. Gaston, K. & Fried, M. CpG methylation has differential effects on the binding of YY1 and ETS proteins to the bi-directional promoter of the Surf-1 and Surf-2 genes. *Nucleic Acids Res.* **23**, 901–909 (1995).
46. Vernon, E. G. & Gaston, K. Myc and YY1 mediate activation of the Surf-1 promoter in response to serum growth factors. *Biochim. Biophys. Acta* **1492**, 172–179 (2000).
47. Mellacheruvu, D. et al. The CRAPome: a contaminant repository for affinity purification-mass spectrometry data. *Nat. Methods* **10**, 730–736 (2013).
48. Madru, C. et al. Chaperoning 5S RNA assembly. *Genes Dev.* **29**, 1432–1446 (2015).
49. Asano, N. et al. Structural and functional analysis of the Rpf2-Rrs1 complex in ribosome biogenesis. *Nucleic Acids Res.* <https://doi.org/10.1093/nar/gkv305> (2015).
50. Kharde, S., Calvino, F. R., Gumiero, A., Wild, K. & Sinning, I. The structure of Rpf2-Rrs1 explains its role in ribosome biogenesis. *Nucleic Acids Res.* <https://doi.org/10.1093/nar/gkv640> (2015).
51. Nieto, B. et al. Efficient fractionation and analysis of ribosome assembly intermediates in human cells. *RNA Biol.* **18**, 182–197 (2021).
52. Wang, M., Anikin, L. & Pestov, D. G. Two orthogonal cleavages separate subunit RNAs in mouse ribosome biogenesis. *Nucleic Acids Res.* **42**, 11180–11191 (2014).
53. Lindström, M. S., Jin, A., Deisenroth, C., Wolf, G. White & Zhang, Y. Cancer-associated mutations in the MDM2 zinc finger domain disrupt ribosomal protein interaction and attenuate MDM2-induced p53 degradation. *Mol. Cell. Biol.* **27**, 1056–1068 (2007).
54. van Riggelen, J., Yetil, A. & Felsher, D. W. MYC as a regulator of ribosome biogenesis and protein synthesis. *Nat. Rev. Cancer* **10**, 301–309 (2010).
55. Russo, A. & Russo, G. Ribosomal proteins control or bypass p53 during Nucleolar Stress. *Int. J. Mol. Sci.* **18**, 140 (2017).
56. Dai, M.-S., Arnold, H., Sun, X.-X., Sears, R. & Lu, H. Inhibition of c-Myc activity by ribosomal protein L11. *EMBO J.* **26**, 3332–3345 (2007).
57. Carotenuto, P., Pecoraro, A., Palma, G., Russo, G. & Russo, A. Therapeutic approaches targeting nucleolus in cancer. *Cells* **8**, 1090 (2019).
58. Howard, G. C. et al. Ribosome subunit attrition and activation of the p53-MDM4 axis dominate the response of MLL-rearranged cancer cells to WDR5 WIN site inhibition. *ELife* **12**, RP90683 (2024).
59. Jansen, J., Bohnsack, K. E., Böhlken-Fascher, S., Bohnsack, M. T. & Dobbelstein, M. The ribosomal protein L22 binds the MDM4 pre-mRNA and promotes exon skipping to activate p53 upon nucleolar stress. *Cell Rep* **43**, 114610 (2023).
60. Ghosh, C., Hu, J. & Kebebew, E. Advances in translational research of the rare cancer type adrenocortical carcinoma. *Nat. Rev. Cancer* **23**, 805–824 (2023).
61. Yin, M. et al. Identification of key genes and pathways in adrenocortical carcinoma: evidence from bioinformatic analysis. *Front. Endocrinol.* **14**, 1250033 (2023).
62. Aspesi, A. et al. Lymphoblastoid cell lines from Diamond Blackfan anaemia patients exhibit a full ribosomal stress phenotype that is rescued by gene therapy. *Sci. Rep.* **7**, 12010 (2017).
63. Le Goff, S. et al. p53 activation during ribosome biogenesis regulates normal erythroid differentiation. *Blood* **137**, 89–102 (2021).
64. Jones, N. C. et al. Prevention of the neurocristopathy Treacher Collins syndrome through inhibition of p53 function. *Nat. Med.* **14**, 125–133 (2008).
65. Vlachos, A., Rosenberg, P. S., Atsidaftos, E., Alter, B. P. & Lipton, J. M. Incidence of neoplasia in Diamond Blackfan anemia: a report from the Diamond Blackfan Anemia Registry. *Blood* **119**, 3815–3819 (2012).
66. Kennedy, A. L. et al. Distinct genetic pathways define pre-malignant versus compensatory clonal hematopoiesis in Shwachman-Diamond syndrome. *Nat. Commun.* **12**, 1334 (2021).
67. Tan, S. et al. Somatic genetic rescue of a germline ribosome assembly defect. *Nat. Commun.* **12**, 5044 (2021).
68. Reilly, C. R. & Shimamura, A. Predisposition to myeloid malignancies in Shwachman-Diamond syndrome: biological insights and clinical advances. *Blood* **141**, 1513–1523 (2023).

69. HaileMariam, M. et al. S-Trap, an ultrafast sample-preparation approach for shotgun proteomics. *J. Proteome Res.* **17**, 2917–2924 (2018).
70. Bouyssié, D. et al. mzDB: A file format using multiple indexing strategies for the efficient analysis of large LC-MS/MS and SWATH-MS data sets *. *Mol. Cell. Proteomics* **14**, 771–781 (2015).
71. Bouyssié, D. et al. Proline: an efficient and user-friendly software suite for large-scale proteomics. *Bioinformatics* **36**, 3148–3155 (2020).
72. Lebaron, S. et al. The ATPase and helicase activities of Prp43p are stimulated by the G-patch protein Pfa1p during yeast ribosome biogenesis. *EMBO J.* **28**, 3808–3819 (2009).
73. Schwanhäusser, B. et al. Global quantification of mammalian gene expression control. *Nature* **473**, 337–342 (2011).

Acknowledgements

We would like to thank the engineers and staff working on the CBI facilities for their great help, as well as Marion Aguirrebengoa for her help with statistical analysis. Funding Ligue Régionale Midi-pyrénées contre le cancer 62339 (S.L.). Ligue National Contre le Cancer, PhD grant (S.T., J.R.). Support from the Ligue National Contre le Cancer « labellisation scheme ». Institut du cancer (INCA), PLBIO022-065, INCA-RESICA (S.L., D.R., Q.P., C.P.C., S.L., V.M. French Ministry of Research (Investissements d’Avenir Program, Proteomics French Infrastructure, ANR-10-INBS-08). INSERM. The CNRS. The University of Toulouse-Paul Sabatier.

Author contributions

Conceptualization: S.L., V.M., C.P.C., J.M., P.E.G., and N.W. Methodology: S.L., V.M., S.T., J.M., C.F., C.P.C., P.E.S., and M.B. Investigation: S.T., P.E.S., J.R., D.R., C.F., M.B., Q.P., S.C., and S.L. Visualization: S.T., P.E.S., C.F., and S.L. Supervision: S.L., C.P.C., V.M., and J.M. Writing—original draft: S.L., V.M., J.M., and C.P.C.

Competing interests

S.T., S.L., V.M., C.P.C., and P.E.G. have filed a patent application on the targeting of SURF2 in cancer, therapies and ribosomopathies treatments. The remaining authors declare no competing interests.

Additional information

Supplementary information The online version contains supplementary material available at <https://doi.org/10.1038/s41467-024-52659-x>.

Correspondence and requests for materials should be addressed to Simon Lebaron.

Peer review information *Nature Communications* thanks the anonymous reviewers for their contribution to the peer review of this work. A peer review file is available.

Reprints and permissions information is available at <http://www.nature.com/reprints>

Publisher’s note Springer Nature remains neutral with regard to jurisdictional claims in published maps and institutional affiliations.

Open Access This article is licensed under a Creative Commons Attribution-NonCommercial-NoDerivatives 4.0 International License, which permits any non-commercial use, sharing, distribution and reproduction in any medium or format, as long as you give appropriate credit to the original author(s) and the source, provide a link to the Creative Commons licence, and indicate if you modified the licensed material. You do not have permission under this licence to share adapted material derived from this article or parts of it. The images or other third party material in this article are included in the article’s Creative Commons licence, unless indicated otherwise in a credit line to the material. If material is not included in the article’s Creative Commons licence and your intended use is not permitted by statutory regulation or exceeds the permitted use, you will need to obtain permission directly from the copyright holder. To view a copy of this licence, visit <http://creativecommons.org/licenses/by-nc-nd/4.0/>.

© The Author(s) 2024